



## RESEARCH ARTICLE

10.1002/2017JD026816

## Special Section:

Deep Convective Clouds and Chemistry 2012 Studies (DC3)

## Key Points:

- For the first time, the RSD variability between two islands (Taiwan and Palau) in western Pacific is studied
- JWD, TRMM, MODIS, and ERA-Interim data sets are used to analyze and understand the RSD variability between Palau and Taiwan
- Orography and aerosols are attributing to RSD variation between two islands in western Pacific

## Correspondence to:

P.-L. Lin,  
tliam@pblap.atm.ncu.edu.tw

## Citation:

Seela, B. K., Janapati, J., Lin, P.-L., Reddy, K. K., Shirooka, R., & Wang, P. K. (2017). A comparison study of summer season raindrop size distribution between Palau and Taiwan, two islands in western Pacific. *Journal of Geophysical Research: Atmospheres*, 122, 11,787–11,805. <https://doi.org/10.1002/2017JD026816>

Received 21 MAR 2017

Accepted 17 OCT 2017

Accepted article online 27 OCT 2017

Published online 11 NOV 2017

©2017. The Authors.

This is an open access article under the terms of the Creative Commons Attribution-NonCommercial-NoDerivs License, which permits use and distribution in any medium, provided the original work is properly cited, the use is non-commercial and no modifications or adaptations are made.

## A Comparison Study of Summer Season Raindrop Size Distribution Between Palau and Taiwan, Two Islands in Western Pacific

Balaji Kumar Seela<sup>1,2</sup> , Jayalakshmi Janapati<sup>1</sup> , Pay-Liam Lin<sup>1</sup> , K. Krishna Reddy<sup>3</sup>, Ryuichi Shirooka<sup>4</sup>, and Pao K. Wang<sup>5,6</sup>

<sup>1</sup>Institute of Atmospheric Physics, Department of Atmospheric Sciences, National Central University, Zhong-Li Region, Tao-Yuan City, Taiwan, <sup>2</sup>Taiwan International Graduate Program, Earth System Science Program, Research Center for Environmental Changes, Academia Sinica, Taipei, Taiwan, <sup>3</sup>Department of Physics, Yogi Vemana University, Kadapa, India, <sup>4</sup>Department of Coupled Ocean-Atmosphere-Land Processes Research, Japan Agency for Marine-Earth Science and Technology, Yokosuka, Japan, <sup>5</sup>Department of Atmospheric and Oceanic Sciences, University of Wisconsin-Madison, Madison, WI, USA, <sup>6</sup>Research Center for Environmental Changes, Academia Sinica, Taipei, Taiwan

**Abstract** Raindrop size distribution (RSD) characteristics in summer season rainfall of two observational sites (Taiwan (24°58'N, 121°10'E) and Palau (7°20'N, 134°28'E)) in western Pacific are studied by using five years of impact type disdrometer data. In addition to disdrometer data, Tropical Rainfall Measuring Mission, Moderate Resolution Imaging Spectroradiometer, and ERA-Interim data sets are used to illustrate the dynamical and microphysical characteristics associated with summer season rainfall of Taiwan and Palau. Taiwan and Palau's raindrop spectra showed a significant difference, with a higher concentration of middle and large drops in Taiwan than Palau rainfall. RSD stratified on the basis of rain rate showed a higher mass-weighted mean diameter ( $D_m$ ) and a lower normalized intercept parameter ( $\log_{10}N_w$ ) in Taiwan than Palau rainfall. Precipitation classification into stratiform and convective regimes showed higher  $D_m$  values in Taiwan than Palau. Furthermore, for both the locations, the convective precipitation has a higher  $D_m$  value than stratiform precipitation. The radar reflectivity-rain rate relations ( $Z = A \cdot R^b$ ) of Taiwan and Palau showed a clear variation in the coefficient and a less variation in exponent values. Terrain-influenced clouds extended to higher altitudes over Taiwan resulted with higher  $D_m$  and lower  $\log_{10}N_w$  values as compared to Palau.

**Plain Language Summary** As the raindrop size distribution (RSD) varies from one location to other location, for the first time, the spatial variability of RSD between two Islands (Taiwan and Palau) in the western Pacific region are studied. A significant RSD differences between Taiwan and Palau are noticed, with more number of small drops in Palau rainfall and more number of middle and large drops in Taiwan rainfall. Both orography and aerosol loading over Taiwan are resulting in more number of middle and large drops over Taiwan as compared to Palau rainfall.

### 1. Introduction

Raindrop size distribution (RSD) information plays a key role in realizing the rain microphysics (Rosenfeld & Ulbrich, 2003), and in quantitative precipitation estimation (QPE) algorithms (Boodoo et al., 2015; Chapon et al., 2008; Ryzhkov & Zrnica, 1995; Seliga & Bringi, 1976). For instance, modeled RSD parameters are used in rainfall estimation algorithms of National Aeronautics and Space Administration (NASA) Tropical Rainfall Measuring Mission (TRMM) Precipitation Radar (PR) (Iguchi et al., 2000; Kozu, Iguchi, et al., 2009; Kozu, Shimomai, et al., 2009) and in Global Precipitation Measurement (GPM) Dual-Precipitation Radar (DPR) (Hou et al., 2008; Liao et al., 2014; Nakamura & Iguchi, 2007). Terrestrial and Earth to space radio links operating at frequencies above 10 GHz depends on the RSD characteristics and their variability (Badron et al., 2011; Chakravarty & Maitra, 2010; Kumar et al., 2010; Marzuki et al., 2009). Knowledge about RSD is essential in improving the microphysics parameterization of numerical cloud models (Cohen & McCaul, 2006; Fadnavis et al., 2014; Gilmore et al., 2004; McFarquhar et al., 2015; Tapiador et al., 2014; Wainwright et al., 2014). Further, RSD plays a pivotal role in the understanding of runoff process, flood hazards control, and in soil erosion studies (Angulo-Martinez & Barros, 2015; Nanko et al., 2016; Rosewell, 1986). Afford mentioned applications of RSD necessitates its extensive study over the globe.

RSD characteristics over a wide range of locations from near-equator to subtropics, subtropics to tropics, high-plains to continental, and oceanic regions were studied by Bringi et al. (2003). They found lower mass-weighted mean diameter values in the maritime-like cluster than the continental-like cluster. RSD characteristics of inland (Gadanki) and maritime continental stations (Singapore and Kototabang) was analyzed by Kozu et al. (2006). They noticed significant seasonal variations in Gadanki, diurnal variations in Kototabang, and with less seasonal/diurnal variations in Singapore. The continental and maritime RSD of northern Brazil was studied by Tenório et al. (2012), and they perceived more small drops ( $< 2$  mm) in the maritime rain than the continental part. Bumke and Seltmann (2012) noticed no systematic differences in RSD of maritime and continental environments over Germany. Ulbrich and Atlas (2007) noticed an increasing trend of median volume diameter ( $D_o$ ) from stratiform to convective regimes of both maritime and continental storms over Brazil. They also found higher median volume diameter and lower normalized intercept parameter in continental storms than maritime storms. With the aid of RSD parameters ( $R$  and  $N_o$ ), Tokay and Short (1996) classified the rainfall into stratiform and convective regimes, and they perceived clear differences in  $Z$ - $R$  relations between stratiform and convective precipitation. Sharma et al. (2009) used ground-based radar and disdrometer to classify the precipitation into convective, transition, and stratiform type. They found bigger drops in stratiform rain events for lower rain rates ( $R < 10$  mm h<sup>-1</sup>) and in convective rain events for higher rain rates ( $R > 10$  mm h<sup>-1</sup>). Tang et al. (2014) analyzed the RSD spatial variability over China, and they found clear regional differences in microphysical parameters of convective precipitation. Recent study of Das et al. (2017) also showed a clear demarcations in the RSD parameters and  $Z$ - $R$  relations among stratiform, convective, and shallow-convective precipitations. With the RSD information, Zwiebel et al. (2016) illustrated the dependency of orography and rain intensity on rainfall structures in different topographic regions (mountain, transition, and plain areas) of southern France. Recently, over southern India, Harikumar (2016) reported more big drops in the orographic rain than nonorographic rain. RSD records over 18 diverse geographical locations around the globe from two-dimensional disdrometer (2-DVD) were compiled by Gatlin et al. (2015). They perceived giant raindrops (diameter  $> 8$  mm) over Colorado, Oklahoma, Huntsville, and they opined that these giant drops are due to melting of hail during their descent. Radhakrishna et al. (2009) studied the seasonal (southwest and northeast monsoon) and spatial (Inland and coastal station) variability of RSD over southern India, and they noticed pronounced seasonal differences at the inland station than the coastal station. The mass-weighted mean diameter values were found to be smaller in coastal station than the inland station. Regional study on RSD characteristics by Marzuki et al. (2013) showed clear demarcations in radar reflectivity-rain rate ( $Z$ - $R$ ) relations among four observational sites in Indonesia. RSD of Equatorial Indian (Gan Island) and West Pacific (Manus Island) Oceans are analyzed by Thompson et al. (2015), and they found analogous RSD between two stations.

So far, in the literature, spatial characteristics of RSD are mostly carried over the inland/coastal regions, or over the oceanic regions (Rangno & Hobbs, 2005), and the RSD spatial variability yet to be documented over the western Pacific region. Henceforth, an attempt has been made to illustrate the summer season RSD differences between two Islands (Palau and Taiwan) in western Pacific by using five years of disdrometer data. These two Islands have different orography, with no terrain over Palau. Taiwan has a central mountain range extending from the north of Island to the south, with a maximum peak of 3,860 m. Such a diverse geography between these two Islands (Palau and Taiwan) allow us to understand the RSD variability between terrains surrounded station to that of the oceanic station. With this brief introduction, section 2 details about the observational sites, data, and methodology. Section 3 illustrates the observational results, and the possible reasons for the variations in RSD characteristics between two sites are detailed in section 4. The results are summarized in section 5.

## 2. Observational Sites, Data, and Methodology

In the present study, five years of RSD measurements from Joss-Waldvogel Disdrometer (JWD) (Joss & Waldvogel, 1969; Waldvogel, 1974) are used to illustrate the RSD characteristics of Taiwan (24°58'N, 121°10'E) and Palau (7°20'N, 134°28'E) in western Pacific region. Figure 1 shows the geographic locations of Taiwan and Palau, and the locations of disdrometer, where the RSD measurements were carried out. The Republic of Palau is an archipelago of about 350 m high and low islands located in the most western part of the Caroline Islands of the southwestern Pacific. To investigate cloud-precipitation processes and air-sea interactions over the warm water pool, Japan Agency for Marine-Earth Science and Technology (JAMSTEC,

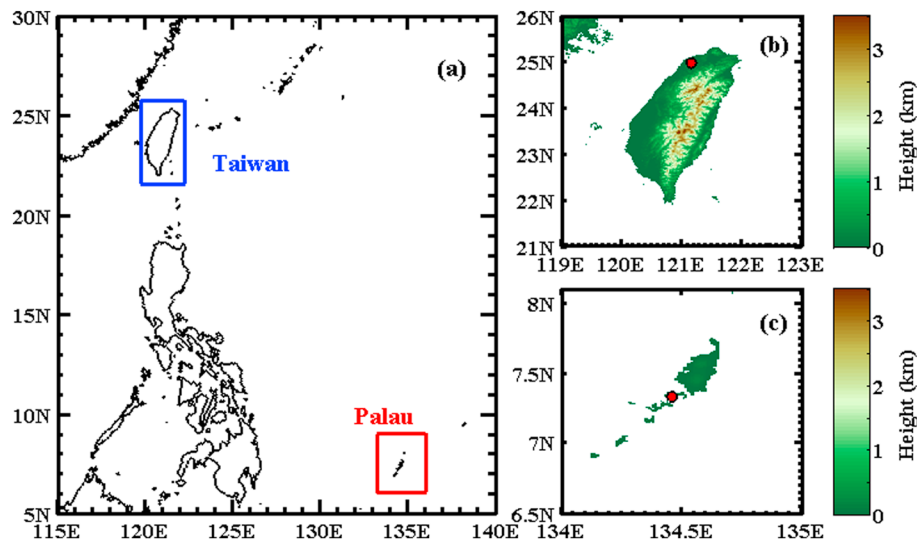


**Figure 1.** (a) Geographical location of Palau and Taiwan in the western Pacific Ocean. (b and c) The red colored circles represent the location of disdrometer.

Japan) carried out a research project (Pacific Area Long-term Atmospheric observation for Understanding of climate change: PALAU) at Palau (Krishna et al., 2016; Kubota et al., 2005; Moteki et al., 2008; Ushiyama et al., 2009). In the present study, the JWD data recorded under this project is used. Taiwan is a subtropical island located southeastern coast of mainland China in the Asia-Pacific conjunction regions. Taiwan is the world's fourth highest island with its central mountain range (CMR) located almost in north-south orientation with an average height of 2 km and maximum peak of nearly 4 km. JWD data recorded at National Central University (NCU) are used in the present study. The disdrometers at Taiwan and Palau were recorded with 1 min sampling interval. Over Taiwan, 16 June to 31 August of each year is considered as summer season (Chen et al., 1999; Chen & Chen, 2003; Kerns et al., 2010). On the basis of wind regimes, Palau has easterly and westerly seasons (Kubota et al., 2005), and the time period from 16 June to 31 August of each year over Palau comes under westerly season. At these two stations (Palau and Taiwan), westerly wind prevails during 16 June to 31 August of each year. Hence, for the RSD comparison between Palau and Taiwan, JWD measurements from 16 June to 31 August of each year are considered from these two (Palau and Taiwan) stations. The JWD data in summer seasons (16 June to 31 August) of the years spanning from 2003 to 2007 and 2004 to 2010 (excluding 2008 and 2009), respectively, for Palau and Taiwan locations are used. During the five years of JWD observations, the RSD measurements due to typhoon rainfall are excluded from the analysis from both Taiwan and Palau station's data.

The JWD is a widely used disdrometer for the measurement of RSD and rain integral parameters. With the help of a Styrofoam cone of cross-sectional area 50 cm<sup>2</sup>, JWD can measure the size of the raindrops ranging from 0.3 to 5.3 mm (Joss & Waldvogel, 1969). Once a raindrop hits the Styrofoam, with its terminal velocity, the diameter of the raindrop can be inferred from the voltage generated by Styrofoam with an accuracy of 5%. Raindrops of diameter ranging from 0.3 to 5.3 mm are separated into 20 channels and the boundaries of each channel increase with drop size from 0.1 to 0.5 mm. Pros and cons of the JWD were well-documented in the literature by the previous researchers (Cao et al., 2008; Joss & Waldvogel, 1969; Lee & Zawadzki, 2005; McFarquhar & List, 1993; Sauvageot & Lacaux, 1995; Sheppard, 1990; Sheppard & Joe, 1994; Tokay et al., 2001; see also <http://www.distromet.com>). In the estimation of raindrop size, the JWD algorithm assumes that the raindrops are falling at terminal velocity in still air. JWD miscalculates the raindrops of diameter less than 1 mm under extremely noisy conditions (heavy rain rate associated with winds) (Tokay et al., 2003). To overcome this problem, manufacturer provided an error correction multiplication matrix based on the correction scheme of Sheppard and Joe (1994). Under intense rainfall events, JWD indicates no drops for the first three to four channels. The multiplicative matrix algorithm does not increase the counts when the channel has no drops (Tokay & Short, 1996). As the dead time correction is not universally utilized within the field (Tokay et al., 2001), in the present study, dead time correction was not applied. To reduce the sampling errors caused by insufficient raw drop counts (< 10 drops), rain rate less than 0.1 mm h<sup>-1</sup> are discarded in the present study (Tokay & Short, 1996).

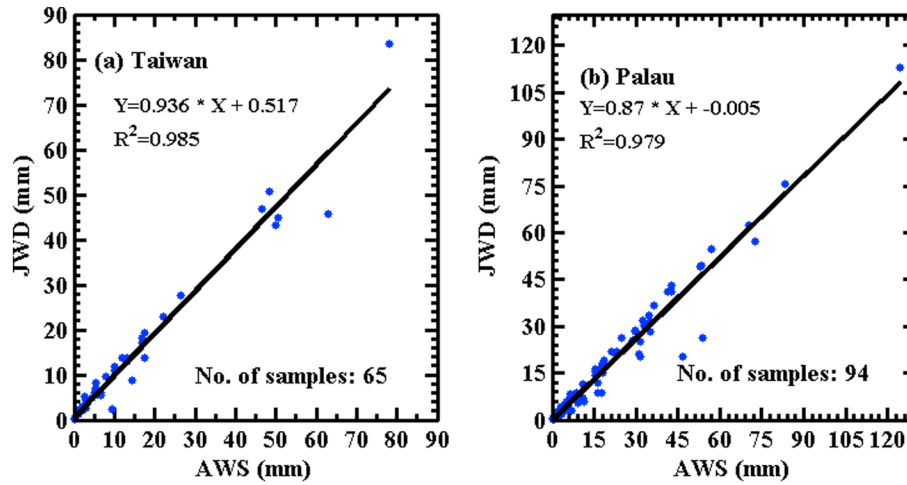


Figure 2. Scatterplot of daily accumulated rainfall measured from disdrometer (JWD) and rain gauge (AWS) for (a) Taiwan and (b) Palau stations.

The raindrop concentration  $N(D)$  ( $m^{-3} mm^{-1}$ ) can be obtained from the JWD measurements by using following equation:

$$N(D) = \sum_{i=1}^{20} \frac{n_i}{A \times \Delta t \times V(D_i) \times \Delta D_i} \quad (1)$$

where  $n_i$  is the number of drops reckoned in the size bin  $i$ ,  $A$  ( $m^2$ ) is sampling area,  $\Delta t$  (s) is the sampling time,  $D_i$  (mm) is the drop diameter for the size bin  $i$ ,  $\Delta D_i$  is the corresponding diameter interval (mm), and  $V(D_i)$  ( $m s^{-1}$ ) is the terminal velocity of the  $i$ th channel raindrops and is estimated from  $V(D_i) = 9.65 - 10.3 \times \exp(-0.6 \times D_i)$  (Gunn & Kinzer, 1949). From the raindrop concentration  $N(D)$ , drop diameter ( $D_i$ ) and terminal velocity  $V(D_i)$ , radar reflectivity factor  $Z$  ( $mm^6 m^{-3}$ ), total number concentration  $N_t$  ( $m^{-3}$ ), and rain rate  $R$  ( $mm h^{-1}$ ) are derived by using the equation

$$Z = \sum_{i=1}^{20} N(D_i) D_i^6 \Delta D_i \quad (2)$$

$$N_t = \sum_{i=1}^{20} N(D_i) \Delta D_i \quad (3)$$

$$R = 6\pi \times 10^{-4} \sum_{i=1}^{20} V(D_i) N(D_i) D_i^3 \Delta D_i \quad (4)$$

Validation of JWDs at both the stations has been carried out by comparing the daily rainfall amounts from their collocated tipping bucket rain gauge of automatic weather station (AWS). The scatterplot of daily rainfall from JWD and the collocated rain gauge for Taiwan and Palau stations are shown in Figure 2. A linear fit is applied to scatterplots of both the stations. From both the figures (Figures 2a and 2b), it is apparent that there is a good correlation between the JWD and rain gauge observations at both the sites. This strongly supports that the JWD measurements at both the locations can be used for the RSD analysis.

The  $n$ th order moment of the drop size distribution is expressed as

$$M_n = \int_{D_{min}}^{D_{max}} D^n N(D) dD \quad (5)$$

here  $n$  stands for the  $n$ th moment of the size distribution.

The mass-weighted mean diameter  $D_m$ , shape parameter  $\mu$ , and slope parameter  $\Lambda$  are evaluated from the 3rd, 4th, and 6th moments of the size distribution.

$$D_m = \frac{M_4}{M_3} \quad (6)$$

The RSD of both the stations are fitted with gamma function as suggested by Ulbrich (1983). The functional form of the gamma distribution is given as

$$N(D) = N_0 D^\mu \exp(-\Lambda D) \quad (7)$$

where  $D$  (mm) is drop diameter,  $N(D)$  ( $m^{-3} mm^{-1}$ ) is number of drops per unit volume per unit size interval,

$N_0$  ( $\text{m}^{-3} \text{mm}^{-1}$ ) is number concentration parameter,  $\mu$  is the shape parameter, and  $\Lambda$  ( $\text{mm}^{-1}$ ) is the slope parameter.

The slope parameter  $\Lambda$  ( $\text{mm}^{-1}$ ) is given by

$$\Lambda = \frac{(\mu + 4)M_3}{M_4} \quad (8)$$

where  $\mu$  is the shape parameter without dimensions and is given by

$$\mu = \frac{(11G - 8) + \sqrt{G(G + 8)}}{2(1 - G)} \quad (9)$$

where  $G = \frac{M_3^2}{M_6 M_3^2}$

The normalized intercept parameter  $N_w$  ( $\text{m}^{-3} \text{mm}^{-1}$ ) is defined by Bringi et al. (2003) as

$$N_w = \frac{4^4}{\pi \rho_w} \left( \frac{10^3 W}{D_m^4} \right) \quad (10)$$

where  $\rho_w$  ( $1.0 \times 10^3 \text{ kg m}^{-3}$ ) represents the density of water and  $W$  ( $\text{kg m}^{-3}$ ) represents the liquid water content for the corresponding size distribution.

The shape parameter ( $\mu$ ) describes the breadth of RSD and determines whether the RSD is of concave downward ( $\mu > 0$ ), upward ( $\mu < 0$ ), or of exponential ( $\mu = 0$ ) shape (Ulbrich, 1983). The slope parameter ( $\Lambda$ ) characterizes the truncation of RSD tail along  $D$ ; small (large)  $\Lambda$  indicates an extension of the RSD tail to larger (smaller)  $D$ . The normalized intercept parameter  $N_w$  represents  $N(D)$  when  $D$  approaches to its minimum value.

Along with the ground-based JWD disdrometer, data sets from Tropical Rainfall Measuring Mission (TRMM) satellite on board Precipitation Radar (PR), Moderate Resolution Imaging Spectroradiometer (MODIS), and European Centre for Medium-Range Weather Forecasts (ECMWF) Interim Re-Analysis (ERA-Interim) are used. Dynamic and thermodynamic characteristics of precipitating clouds over Taiwan and Palau are tried to understand with the help of storm and bright band heights from 2A23 data product of TRMM-PR, cloud effective radii (CER) of ice, water droplets from MODIS, and convective available potential energy (CAPE) from ERA-Interim. The TRMM PR was operated with 13.8 GHz frequency at 4.3 km/5 km horizontal resolution over a 215 km/247 km swath during preboost (before 7 August 2001)/postboost (after 24 August 2001) covering the tropical region from 37°S to 37°N. TRMM-PR algorithm instruction manual for version 7 provides the detailed description of 2A23 data product and its algorithm. For further details, please refer to Awaka et al. (1997, 1998, 2009), Iguchi et al. (2000), and Kummerow et al. (2001). In addition to this, CER of ice and water particles from MODIS data product, MOD08\_D3, are used. The MOD08\_D3 data product available at  $1^\circ \times 1^\circ$  spatial resolution is interpolated to  $0.125^\circ \times 0.125^\circ$ . The cloud effective radii (CER) are the area weighted mean radius of cloud droplets and can be inferred from the multiwavelength reflected solar radiation measurements (King et al., 2003; Nakajima & King, 1990; Platnick et al., 2003). The level 3 data product provides atmospheric parameters related to aerosol particle properties, water vapor, and cloud optical and physical properties (Remer et al., 2005). Multispectral reflectance method is used to retrieve the CER for liquid and ice phases (Nakajima & King, 1990). More details about the cloud product algorithms of MODIS are documented by Platnick et al. (2003) and King et al. (2003). Also, the daily mean values of convective available potential energy (CAPE,  $\text{J kg}^{-1}$ ) with a grid resolution of  $0.125^\circ \times 0.125^\circ$  are taken from ERA-Interim (Dee et al., 2011). In this study, the daily mean data products of ERA-interim, TRMM-PR, and MODIS are considered for the JWD measured summer season (16 June to 31 August) rainy days (2003–2007 for Palau, 2004–2007, 2010 for Taiwan; excluding typhoon rainy days) over Taiwan and Palau stations.

### 3. Observational Results

During five years of observations, a total number of 65 rainy days (7,466 min of raindrop spectra) over Taiwan, and 112 rainy days (18,868 min of raindrop spectra) over Palau were observed with the JWD. Figure 3a shows the variation of number of raindrops per unit volume per diameter range,  $N(D)$  ( $\text{m}^{-3} \text{mm}^{-1}$ ), with raindrop size,  $D$  (mm), for summer season precipitation of Taiwan and Palau. The mean raindrop concentration,

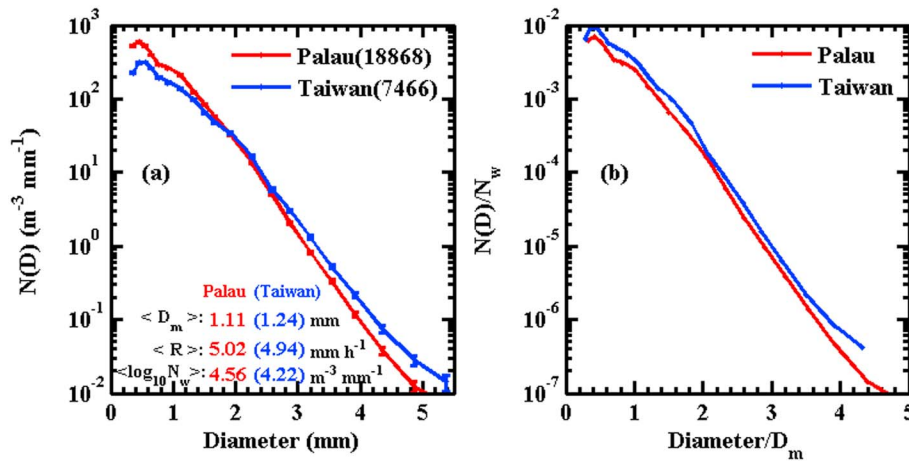


**Figure 3.** (a) Variation of mean raindrop concentration ( $N(D)$ ,  $m^{-3} mm^{-1}$ ) with drop diameter ( $D$ , mm) in summer season rainfall of Taiwan and Palau, and (b) normalized gamma distribution of Taiwan and Palau rainfall. The numbers in the legend parenthesis of Figure 3a indicate the total number of samples over Taiwan and Palau stations. The mean RSD parameters (represented with angles brackets  $\langle \rangle$ ) of Palau and Taiwan rainfall are also shown in Figure 3a. The error bars in Figure 3a represents the standard error of each channel samples.

$N(D)$  ( $m^{-3} mm^{-1}$ ), is obtained from the rainy samples of Taiwan (7,466 samples) and Palau (18,868 samples) and are shown with blue and red colors, respectively, in Figure 3a. In the present study, raindrop diameter classification (small, middle, and large size drops) proposed by previous researchers (Jayalakshmi & Reddy, 2014; Krishna et al., 2016; Narayana Rao et al., 2009; Tokay et al., 2008) is adapted to explain the RSD variations. Raindrops of diameter less than 1 mm are considered as small drops, 1 to 3 mm as middle-size drops, and above 3 mm as large drops. An inspection of raindrop spectra in Figure 3a shows that the concentration of raindrops below 2 mm diameter is higher at Palau in comparison to Taiwan rainfall. A similar type of finding was reported by Tenório et al. (2012) over eastern Brazil. They found a higher concentration of small drops ( $< 2$  mm) in maritime rainfall than continental rainfall. As the raindrop concentration depends on rain rate, it is hard to make reliable interpretation of differences between unnormalized spectra of Taiwan and Palau rainfall (as in Figure 3a). As a result, normalization procedure of Testud et al. (2001) is adopted to the RSD of Taiwan and Palau rainfall. As this procedure does not depend on the shape of the observed raindrop spectra, it can be useful in comparing the RSD of different precipitations and also for inspecting them for indications of differences in the physical processes that produce the rain. The drop diameter ( $D$ , mm) and raindrop concentration ( $N(D)$ ,  $m^{-3} mm^{-1}$ ) of Taiwan and Palau are normalized with the mass-weighted mean diameter ( $D_m$ , mm) and normalized intercept parameter ( $N_w$ ,  $m^{-3} mm^{-1}$ ), respectively, and are shown in Figure 3b. From the figure, it is apparent that the normalized spectra of Taiwan depart from the Palau spectra.

### 3.1. Raindrop Size Distribution in Different Rain Rate Classes

In order to demonstrate the differences in Palau and Taiwan RSD, both the station's rainfall are divided into 12 rain rate classes (C1: 0.1–0.2, C2: 0.2–0.4, C3: 0.4–0.7, C4: 0.7–1, C5: 1–2, C6: 2–5, C7: 5–8, C8: 8–12, C9: 12–18, C10: 18–25, C11: 25–40, and C12:  $>40$   $mm h^{-1}$ ). These rain rate classes are chosen in such a way that the mean rain rate in each class is nearly equal in both the stations and the number of data points are sufficiently large in each class. A similar classification criterion was adopted by previous researchers (Jayalakshmi & Reddy, 2014; Krishna et al., 2016; Narayana Rao et al., 2009); however, they considered different rain rate classes. Table 1 summarizes the rain rate statistics of both the stations. Figure 4 shows the variation of number of raindrops per unit volume per diameter range,  $N(D)$  ( $m^{-3} mm^{-1}$ ), with raindrop size,  $D$  (mm), for each rain rate class of Taiwan and Palau rainfall. For the first two rain rate classes (Figures 4a and 4b; C1: 0.1–0.2, C2: 0.2–0.4  $mm h^{-1}$ ) rain drops below 0.6 mm are more in Palau rainfall than Taiwan rainfall. For the next three rain rate classes (Figures 4c–4e; C3: 0.4–0.7, C4: 0.7–1, C5: 1–2  $mm h^{-1}$ ), concentration of small drops (diameter  $< 1$  mm) is higher in Palau rainfall than Taiwan rainfall, and a reverse pattern can be seen for middle and large raindrops (diameter  $> 1$  mm). Raindrops below 1.3 mm and 1.5 mm diameter

**Table 1**  
Statistical Measure of Disdrometer-Derived Rain Rate Classes for Taiwan and Palau Rainfall

Rain rate threshold	Rain rate class	Taiwan						Palau					
		No. of samples	$R_{max}$ (mm h <sup>-1</sup> )	Mean (mm h <sup>-1</sup> )	SD	Skewness	Kurtosis	No. of samples	$R_{max}$ (mm h <sup>-1</sup> )	Mean (mm h <sup>-1</sup> )	SD	Skewness	Kurtosis
0.1 < R < 0.2	C1	1,110	0.20	0.15	0.03	0.22	1.85	2,523	0.20	0.14	0.03	0.25	1.87
0.2 < R ≤ 0.4	C2	1,139	0.40	0.29	0.06	0.15	1.79	2,786	0.40	0.29	0.06	0.24	1.86
0.4 < R ≤ 0.7	C3	977	0.70	0.54	0.08	0.21	1.87	2,187	0.70	0.53	0.09	0.20	1.88
0.7 < R ≤ 1	C4	562	1.00	0.84	0.08	0.17	1.90	1,373	1.00	0.84	0.09	0.07	1.80
1 < R ≤ 2	C5	1,024	2.00	1.45	0.29	0.26	1.81	2,752	2.00	1.45	0.29	0.19	1.80
2 < R ≤ 5	C6	<b>1,201</b>	5.00	3.19	0.84	0.42	2.04	<b>3,257</b>	5.00	3.23	0.86	0.35	1.97
5 < R ≤ 8	C7	431	7.97	6.30	0.84	0.18	1.90	1,204	8.00	6.31	0.85	0.28	1.93
8 < R ≤ 12	C8	255	12.00	9.69	1.15	0.32	1.95	771	12.00	9.80	1.15	0.20	1.83
12 < R ≤ 18	C9	194	17.95	15.00	1.65	-0.08	1.85	672	18.00	14.65	1.71	0.22	1.91
18 < R ≤ 25	C10	175	24.98	21.26	2.08	0.20	1.73	406	24.99	21.07	1.96	0.24	1.94
25 < R ≤ 40	C11	195	39.96	31.77	4.30	0.17	1.96	461	39.93	31.30	4.22	0.30	1.94
R > 40	C12	203	<b>109.26</b>	<b>59.39</b>	<b>15.81</b>	<b>1.33</b>	<b>4.54</b>	476	<b>135.09</b>	<b>60.29</b>	<b>17.41</b>	<b>1.22</b>	<b>4.55</b>
Total		7,466	109.26	4.94	11.38	4.25	24.81	18,868	135.09	5.02	11.17	4.48	28.06

Note. The numbers reported in bold indicate the maximum values in each column.

have higher concentration in Palau rainfall than Taiwan rainfall and raindrops above 1.3 mm and 1.5 mm diameter have slightly higher concentration in Taiwan than Palau rainfall for the sixth (C6:  $2 \leq R < 5 \text{ mm h}^{-1}$ ) and seventh (C7:  $5 \leq R < 8 \text{ mm h}^{-1}$ ) rain rate classes, respectively. Raindrops of diameter greater than 1.9 mm have a higher concentration in Taiwan rainfall as compared to Palau rainfall in the eighth and ninth rain rate classes (Figures 4h and 4i; C8: 8–12, C9: 12–18  $\text{mm h}^{-1}$ ). Raindrops of diameter greater than 2 mm have a higher concentration in Taiwan rainfall when compared to Palau rainfall for the two following rain rate classes (Figures 4j and 4k; C10: 18–25, C11: 25–40  $\text{mm h}^{-1}$ ). In the last rain rate class (Figure 4l; C12:  $>40 \text{ mm h}^{-1}$ ) the concentration of large drops is higher in Taiwan than Palau rainfall. To look into the RSD variations in these 12 rain rate classes for a given location, the RSD of 12 rain rate classes are redrawn separately for Taiwan and Palau and are shown in Figure 5. From Figure 5 we can see that the raindrop concentration of middle and large drops ( $> 1 \text{ mm}$ ) is increasing with the increase of rain rate class (from C1 to C12) for both Taiwan and Palau stations. For the first six rain rate classes (C1–C6) there is no much decrease of very small drops ( $< 0.5 \text{ mm}$ ) with the increase of rain rate class. However, for the rest of the six rain rate classes (C7–C12), the concentration of small drops ( $< 1 \text{ mm}$ ) is decreasing with the increase in rain rate class.

To further emphasize the clear differences in RSD characteristics between Palau and Taiwan rainfall, a percentage parameter  $\delta(D, R)$  is considered. The  $\delta(D, R)$  is the ratio of a raindrop concentration in one location ( $N(D)$  of Taiwan/Palau) at a diameter  $D$  and rain rate  $R$  to the sum of the raindrop concentrations in both the locations ( $N(D)$  of Taiwan and Palau). The percentage parameter chosen in the present study is alike to Radhakrishna et al. (2009). However, we used different rain rate classes. Variations in  $\delta(D, R)$  of Palau and Taiwan rainfall are depicted in Figure 6. From the figure, we can notice distinct variations in raindrop concentration of Taiwan and Palau rainfall. The contribution of small drops ( $< 1 \text{ mm}$  diameter) is predominant in Palau than Taiwan (except in the last rain rate class), whereas the contribution of middle and large drops ( $> 2 \text{ mm}$ ) is higher in Taiwan as compared to Palau rainfall.

The RSDs of both the stations are fitted to the gamma distribution. Variations in mass-weighted mean diameter ( $D_m$ ) and gamma parameters ( $\log_{10}N_w$ ,  $\mu$ , and  $\Lambda$ ) with rain rate classes are shown in Figure 7. At both the sites, mean  $D_m$  increases with the increase in rain rate class (Figure 7a), which is caused by the increase of large drops and decrease of small drops with the increase in rain rate. This feature is consistent with the results of previous researchers (Jayalakshmi & Reddy, 2014; Krishna et al., 2016; Narayana Rao et al., 2009; Rosenfeld & Ulbrich, 2003; Testud et al., 2001). Mean  $D_m$  values of Palau rainfall are relatively lower than Taiwan rainfall. Higher  $D_m$  values of Taiwan are due to the relatively large number of middle and large drops as compared to Palau rainfall. The mean  $D_m$  value varies between 0.88 and 2.12 mm in Taiwan, and it ranges from 0.78 to 2.06 mm in Palau. The difference in mean  $D_m$  between Taiwan and Palau rainfall varied from 0.06 to 0.23 mm. An increasing trend in mean normalized intercept parameter  $\log_{10}N_w$  can be seen for both Taiwan and Palau rainfall (Figure 7b). The mean normalized intercept parameter ( $\log_{10}N_w$ ,  $\text{m}^{-3} \text{ mm}^{-1}$ ) ranges from 4.08 to 4.56 in Taiwan rainfall whereas it varies from 4.39 to 4.78 in Palau rainfall. The mean value of  $\log_{10}N_w$  is lower in Taiwan rainfall when compared to Palau rainfall. In both the locations (Palau, Taiwan) the shape parameter ( $\mu$ ,  $-$ ) shows an irregular decreasing trend with the increase in rain rate class (Figure 7c). Mean  $\mu$  values vary from 4.58 to 10.05, and from 5.91 to 13.11, respectively, in

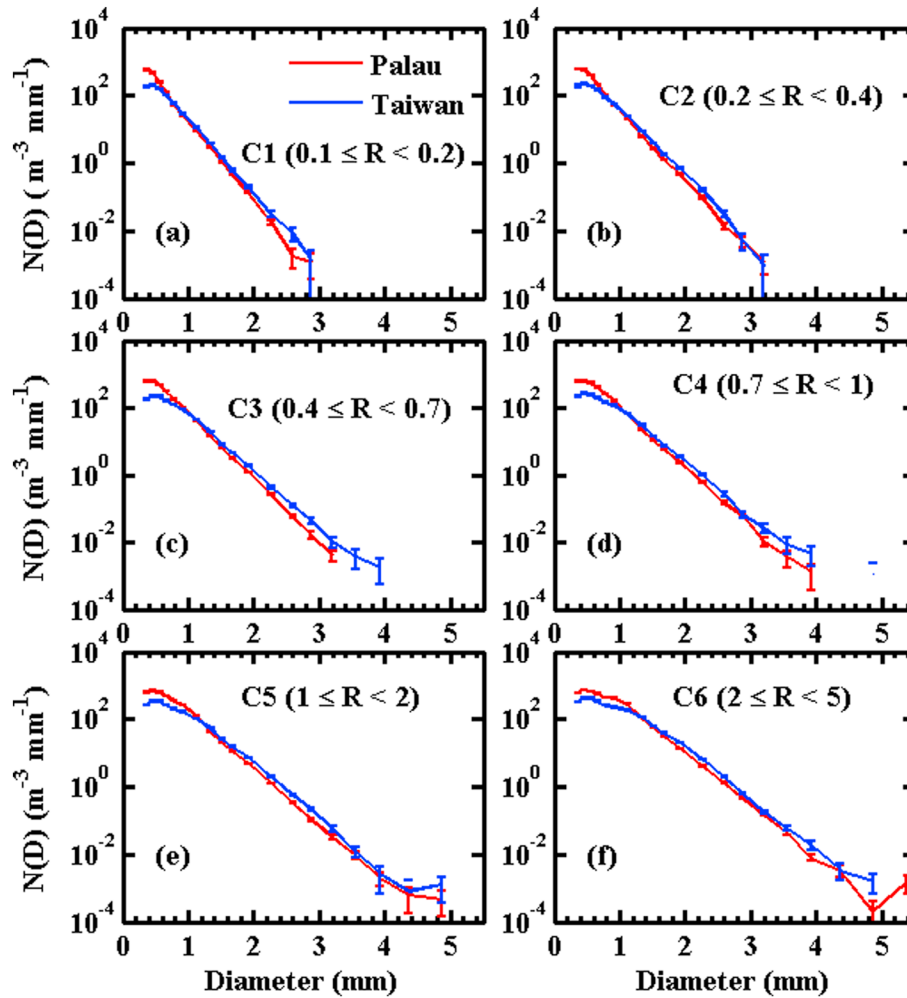


**Figure 4.** Average raindrop spectra of Taiwan (blue color) and Palau (red color) rainfall in 12 rain rate classes (C1: 0.1–0.2, C2: 0.2–0.4, C3: 0.4–0.7, C4: 0.7–1, C5: 1–2, C6: 2–5, C7: 5–8, C8: 8–12, C9: 12–18, C10: 15–25, C11: 25–40, and C12: >40 mm h<sup>-1</sup>). The error bars in each subplot represents the standard error of each channel samples.

Taiwan and Palau rainfall. On the other hand, mean slope parameter ( $\Lambda$ , mm<sup>-1</sup>) shows a decreasing trend with the increase in rain rate at both the stations (Palau and Taiwan) (Figure 7d). In all rain rate classes (C1–C12), the mean slope parameter is higher in Palau when compared to Taiwan. In Taiwan rainfall, the mean values of  $\Lambda$  varied from 4.64 to 16.39 m<sup>-1</sup>, whereas in Palau rainfall, it changes from 5.36 to 19.08 m<sup>-1</sup>. Table 2 shows the statistical values of  $D_m$ ,  $N_w$ ,  $\mu$ , and  $\Lambda$  of Palau and Taiwan rainfall in 12 rain rate classes. In all rain rate classes, Palau rainfall has higher values of  $N_w$ ,  $\mu$ , and  $\Lambda$  and Taiwan rainfall has higher  $D_m$  values. Similar type of results were reported by Jung et al. (2012) for a squall line in south Taiwan. They found higher (lower) values of  $D_m$  ( $N_w$ ,  $\mu$ , and  $\Lambda$ ) in convective region of the Taiwan squall line than tropical oceanic storms.

### 3.2. RSD Variations in Stratiform and Convective Precipitation

It is clearly evident from the literature (Niu et al., 2010; Sharma et al., 2009; Thurai et al., 2016; Tokay et al., 2008; Tokay & Short, 1996) that the RSD in stratiform precipitation significantly vary from convective precipitation. With the help of changes in RSD parameters during convective and stratiform precipitation, Ulbrich and Atlas (2007) argued to use different Z-R relations in stratiform and convective precipitation. Bringi et al. (2003) studied the variations in  $D_m$  and  $N_w$  values in stratiform and convective rainfall of different climatic regions by using two different disdrometers. Sequential variations in RSD parameters from

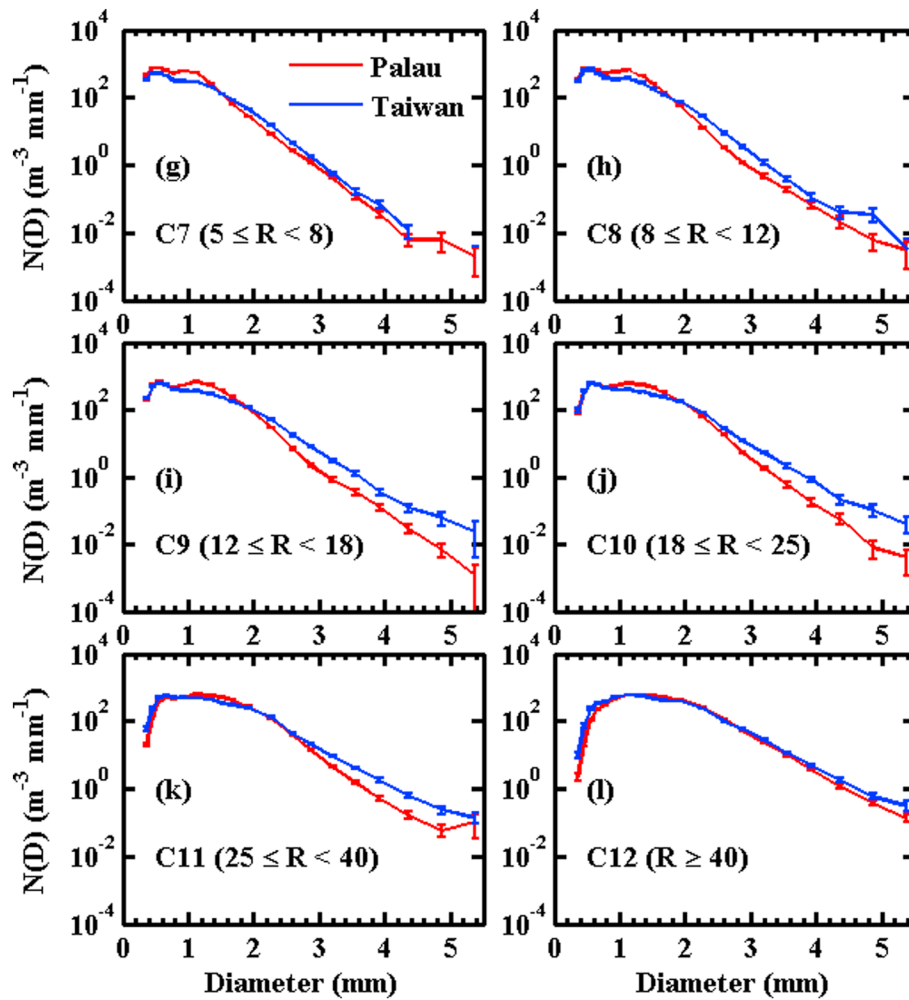


Figure 4. (continued)

convective to stratiform precipitations was demonstrated by Tokay and Short (1996). As the dynamical and microphysical properties of stratiform and convective precipitations were found to vary (Tokay & Short, 1996), we analyzed the RSD of Taiwan and Palau rainfall by classifying into stratiform and convective regimes. With the help of different ground-based instruments (disdrometer, profiler, and radar), different researchers

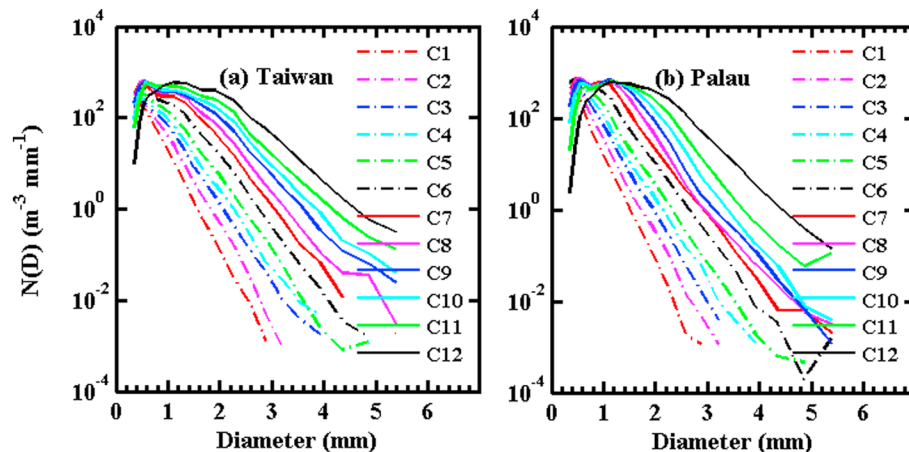
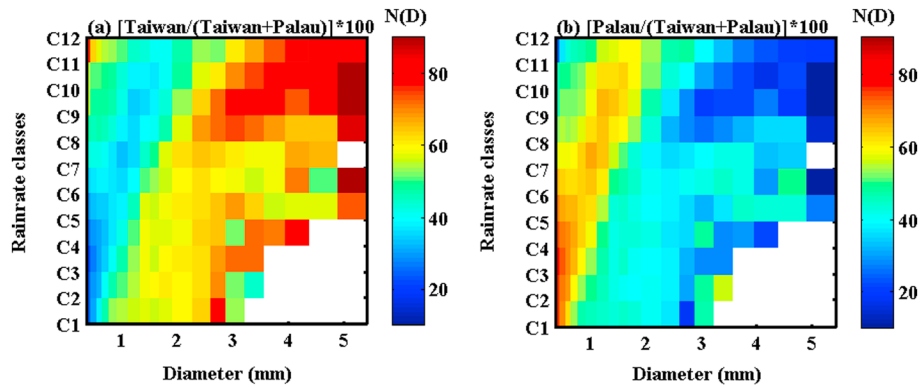
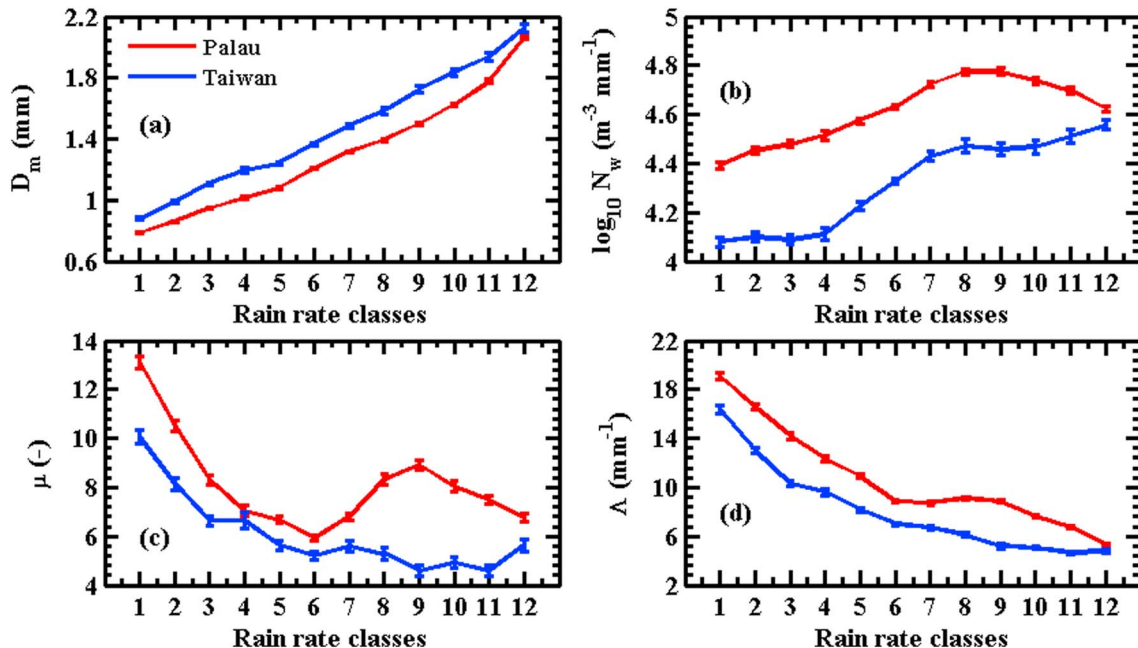


Figure 5. Average raindrop spectra of (a) Taiwan and (b) Palau rainfall in 12 rain rate classes.



**Figure 6.** Percentage parameter,  $\delta(D, R)$  for (a) Taiwan and (b) Palau rainfall. As the above figures (Figures 5a and 5b) are drawn with pcolor command in MATLAB, the number of grid spaces in y axis are one fewer than the number of rain rate classes.

adopted different rain classification criteria (Bringi et al., 2003; Krishna et al., 2016; Narayana Rao et al., 2001; Steiner et al., 1995; Thurai et al., 2016; Tokay & Short, 1996; Williams et al., 1995). In the present study, we have categorized the Taiwan and Palau rainfall into stratiform and convective regimes by using classifications criteria proposed by Bringi et al. (2003). Bringi et al. (2003) separated the rainfall into stratiform and convective rain type by using standard deviation of rain rate ( $\sigma_R$ ) over five consecutive 2 min RSD samples. The classification criteria was based on rain rate ( $R \geq 0.5 \text{ mm h}^{-1}$  and  $\sigma_R \leq 1.5 \text{ mm h}^{-1}$  for stratiform rain and  $R \geq 5.0 \text{ mm h}^{-1}$  and  $\sigma_R > 1.5 \text{ mm h}^{-1}$  for convective rain. In the present study, Palau and Taiwan rainfall are separated into stratiform and convective type by using 10 consecutive 1 min RSD samples. Figure 8 depicts the RSD variations in convective and stratiform rainfall of both the stations. In Palau rainfall, drop concentration of convective regime is higher than the stratiform regime for the drops above 0.5 mm diameter (Figure 8a). From the Figure 8b, it is apparent that the convective rainfall of Taiwan has a higher drop concentration to that of stratiform rainfall for the raindrops of all sizes. The convective regimes of both Taiwan and Palau rainfall showed a broad distribution with a concave downward shape (at 1.2 mm) as compared to stratiform regimes. This behavior is partly due to the association of convective rainfall with



**Figure 7.** Distribution of (a) mass-weighted mean diameter ( $D_m$ , mm), (b) normalized intercept parameter ( $\log_{10} N_w$ ,  $\text{m}^{-3} \text{ mm}^{-1}$ ), (c) shape ( $\mu$ ,  $-$ ), and (d) slope ( $\Lambda$ ,  $\text{mm}^{-1}$ ) parameter of Palau (red color) and Taiwan (blue color) rainfall with respect to rain rate.

**Table 2**  
Mean and Standard Deviation Values of  $D_m$ ,  $\log_{10}(N_w)$ ,  $\mu$ , and  $\Lambda$  for Taiwan and Palau Rainfall in Different Rain Rate Classes

Rain rate class	Taiwan								Palau							
	$D_m$		$\log_{10}N_w$		$\mu (-)$		$\Lambda (mm^{-1})$		$D_m$		$\log_{10}N_w$		$\mu (-)$		$\Lambda (mm^{-1})$	
	Mean	SD	Mean	SD	Mean	SD	Mean	SD	Mean	SD	Mean	SD	Mean	SD	Mean	SD
C1	0.88	0.23	4.08	<b>0.63</b>	<b>10.05</b>	<b>9.77</b>	<b>16.39</b>	<b>11.76</b>	0.78	0.25	4.39	<b>0.76</b>	<b>13.11</b>	<b>12.88</b>	<b>19.08</b>	<b>14.08</b>
C2	0.99	0.27	4.10	<b>0.63</b>	8.14	8.21	13.01	9.32	0.86	0.27	4.45	0.74	10.52	11.29	16.59	12.97
C3	1.11	0.30	4.09	0.60	6.63	6.86	10.27	7.06	0.95	0.27	4.48	0.69	8.31	8.83	14.18	11.33
C4	1.19	0.34	4.11	0.61	6.65	7.69	9.60	7.36	1.01	0.29	4.51	0.66	7.04	7.62	12.32	9.83
C5	1.24	0.29	4.23	0.52	5.64	6.19	8.15	5.34	1.08	0.29	4.58	0.59	6.66	7.68	10.89	8.50
C6	1.37	0.27	4.33	0.44	5.19	5.23	7.02	4.29	1.21	0.27	4.63	0.49	5.91	6.42	8.87	6.12
C7	1.49	0.27	4.43	0.39	5.59	4.83	6.70	3.58	1.32	0.28	4.72	0.45	6.80	5.47	8.72	4.69
C8	1.58	0.30	4.47	0.42	5.27	4.00	6.13	3.01	1.39	0.24	4.77	0.35	8.33	5.55	9.10	4.09
C9	1.72	0.31	4.46	0.36	4.58	3.21	5.19	2.38	1.50	0.23	<b>4.78</b>	0.32	8.92	4.74	8.86	3.47
C10	1.83	0.34	4.47	0.36	4.91	2.92	5.06	2.00	1.62	0.22	4.74	0.28	8.04	4.26	7.63	3.03
C11	1.94	<b>0.37</b>	4.51	0.36	4.59	2.92	4.64	1.97	1.78	<b>0.30</b>	4.70	0.29	7.47	3.61	6.72	2.56
C12	<b>2.12</b>	0.33	<b>4.56</b>	0.29	5.63	3.74	4.77	2.34	<b>2.06</b>	<b>0.30</b>	4.62	0.25	6.76	3.65	5.36	1.88
Total	1.24	0.41	4.22	0.56	6.72	7.11	9.80	8.08	1.11	0.39	4.56	0.62	8.37	8.94	12.19	10.27

Note. The numbers reported in bold indicate the maximum values in each column.

collisional breakup of large drops (Hu & Srivastava, 1995). However, in both Taiwan and Palau rainfall, an exponential distribution can be seen in stratiform regimes, with relatively less tendency toward downward concavity. Previous researcher reported the similar findings for the stratiform and convective regimes (Chen et al., 2013; Jayalakshmi & Reddy, 2014; Krishna et al., 2016; Niu et al., 2010). To further look into the variations between Taiwan and Palau rainfall for a given rain type, the RSD of Taiwan and Palau rainfall for stratiform and convective regimes are separately drawn in Figures 8c and 8d, respectively. From the Figures 8c and 8d, it is clearly evident that the raindrops of diameter less than 1.2 mm are in higher concentration for Palau rainfall as compared to Taiwan rainfall for stratiform precipitation, whereas raindrops above 2 mm diameter are more in Taiwan than Palau for the convective regime.

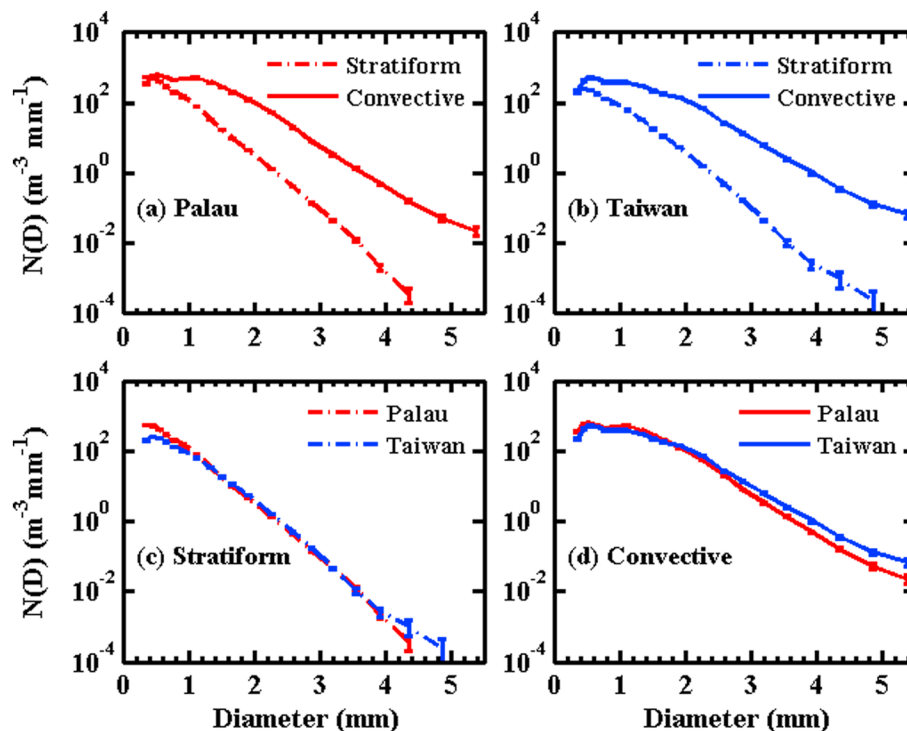


**Figure 8.** Variation of raindrop concentration with rain type in summer season precipitations of Taiwan and Palau.

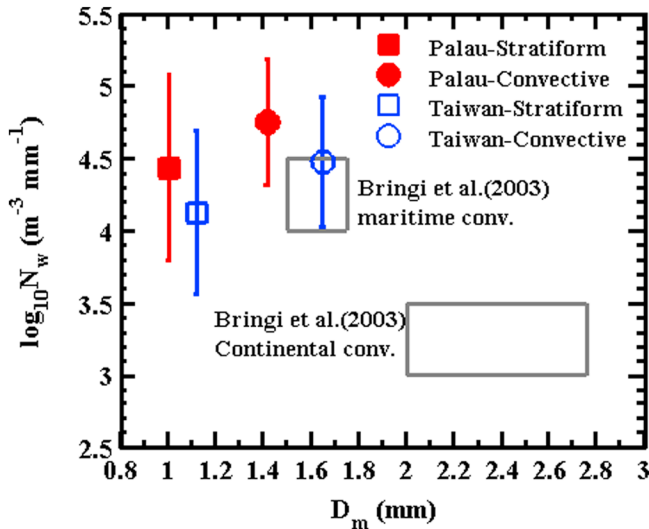


**Figure 9.** Variations of average mass-weighted mean diameter ( $D_m$ ) with normalized intercept parameter ( $\log_{10}N_w$ ) (along with plus-minus standard deviation) for stratiform and convective regimes of Palau and Taiwan rainfall.

Figure 9 shows the variations of mass-weighted mean diameter ( $D_m$ , mm) and normalized intercept parameter ( $\log_{10}N_w$ ,  $m^{-3} mm^{-1}$ ) in stratiform and convective regimes of Taiwan and Palau rainfall. From the figure, it is apparent that the convective precipitations have relatively higher  $D_m$  values than stratiform precipitations. On the other hand, Taiwan rainfall has a higher  $D_m$  and lower  $\log_{10}N_w$  values than Palau rainfall for both the rainfall regimes (stratiform and convective). Table 3 provides the mean and standard deviation values of  $R$ , LWC,  $D_{max}$ ,  $\log_{10}N_t$ ,  $D_m$ ,  $\log_{10}N_w$ ,  $\mu$ , and  $\Lambda$  for stratiform and convective regimes of Taiwan and Palau rainfall. Bringi et al. (2003) measured  $\log_{10}N_w$  and  $D_m$  values for a wide range of locations (from near equator to subtropics, subtropics to tropics, oceanic, and high plains to continental). For convective rain, they found  $D_m$  ( $\log_{10}N_w$ ) ranging from 1.5 to 1.75 mm (4 to 4.5  $m^{-3} mm^{-1}$ ) for the maritime-like cluster and 2 to 2.75 mm (3 to 3.5  $m^{-3} mm^{-1}$ ) for the continental-like cluster. Comparison of current results with the Bringi et al. (2003) suggests that the RSDs at both Taiwan and Palau sites are similar to the maritime-like convective RSD. Nevertheless, it is somewhat interesting for Palau, where the environment seems to be more maritime than Taiwan. The RSD parameters from convective precipitation of Palau rainfall are deviated from the maritime-like ones, whereas Taiwan's RSD parameters are similar to the maritime-like parameters. This result would suggest that the continental/maritime classification of RSD is not necessarily applied to convective precipitation over the western Pacific region.

precipitation of Palau rainfall are deviated from the maritime-like ones, whereas Taiwan's RSD parameters are similar to the maritime-like parameters. This result would suggest that the continental/maritime classification of RSD is not necessarily applied to convective precipitation over the western Pacific region.

### 3.3. Radar Reflectivity (Z)-Rain Rate (R) Relations

The uncertainties in the estimation of rainfall from radars can be minimized by utilizing proper radar reflectivity-rain rate ( $Z$ - $R$ ) relations (Battan, 1973; Chapon et al., 2008; Raghavan, 2003). These  $Z$ - $R$  relations were found to vary from season to season, one climatic region to the other, and even in different precipitation type (Atlas et al., 1999; Marzuki et al., 2013; Tokay & Short, 1996; Ulbrich & Atlas, 2007). The coefficient ( $A$ ) of  $Z$ - $R$  relations ( $Z = A \cdot R^b$ ) infers the presence of smaller or bigger raindrops, and the exponent " $b$ " infers microphysical processes. If the exponent is equivalent to unity ( $b \sim 1$ ), the RSD evolves from number controlled process under steady and equilibrium rainfall. Whereas if the exponent is greater than unity

**Table 3**

Mean and Standard Deviation of  $R$ , LWC,  $D_{max}$ ,  $\log_{10}N_t$ ,  $D_m$ ,  $\log_{10}N_w$ ,  $\mu$ , and  $\Lambda$  for Stratiform and Convective and Total Rainfall of Taiwan and Palau Stations

Parameters		Taiwan			Palau		
		Stratiform	Convective	Total	Stratiform	Convective	Total
$R$ (mm h <sup>-1</sup> )	Mean	1.01	<b>19.40</b>	4.94	1.10	16.91	5.02
	SD	1.10	<b>19.46</b>	11.38	1.18	18.83	11.17
LWC (g m <sup>-3</sup> )	Mean	0.03	<b>0.56</b>	0.14	0.03	0.49	0.14
	SD	0.03	<b>0.56</b>	0.33	0.03	0.54	0.32
$D_{max}$ (mm)	Mean	1.88	<b>3.10</b>	2.16	1.74	2.58	1.94
	SD	0.59	<b>0.94</b>	0.84	0.63	0.88	0.79
$\log_{10}N_t$ (m <sup>-3</sup> )	Mean	146.75	576.27	250.10	253.33	<b>682.90</b>	392.14
	SD	141.51	<b>317.57</b>	261.65	249.07	316.14	339.67
$D_m$ (mm)	Mean	1.12	<b>1.65</b>	1.24	1.01	1.42	1.11
	SD	0.32	<b>0.45</b>	0.41	0.30	0.44	0.39
$\log_{10}N_w$ (m <sup>-3</sup> mm <sup>-1</sup> )	Mean	4.12	4.47	4.22	4.43	<b>4.75</b>	4.56
	SD	0.56	0.45	0.56	<b>0.64</b>	0.43	0.62
$\mu$ (-)	Mean	4.14	5.10	5.19	4.09	<b>7.84</b>	7.67
	SD	4.42	3.68	3.92	4.04	4.57	<b>5.13</b>
$\Lambda$ (mm <sup>-1</sup> )	Mean	5.42	5.48	5.65	6.00	<b>7.95</b>	8.08
	SD	3.01	2.77	2.93	3.92	3.58	<b>3.94</b>

Note. The numbers reported in bold indicate the maximum values in each row.

**Table 4**  
Radar Reflectivity-Rain Rate ( $Z = A \cdot R^b$ ) Relations for Taiwan and Palau Rainfall

Precipitation type	Taiwan	Palau
Stratiform	$Z = 299.55 R^{1.38}$	$Z = 226.61 R^{1.39}$
Convective	$Z = 256.82 R^{1.37}$	$Z = 163.2 R^{1.41}$
Total	$Z = 283.35 R^{1.35}$	$Z = 203.28 R^{1.34}$

table, a clear variation in coefficient and a less variation in exponent values can be noticed between Taiwan and Palau rainfall. It was well understood that if we used single tropical Z-R relations ( $Z = 250 R^{1.2}$ ), the precipitation might be underestimated at one location or overestimated at another location (Atlas & Williams, 2003; Baeck & Smith, 1998). Current results reconfirm the opinion of the previous researcher. Hence, there is a need to adopt the modified Z-R relations in obtaining rainfall at these two stations by QPE.

#### 4. Discussion

Taiwan has a typical geographical area with its CMR aligned almost in north-south direction (Figure 1b), whereas the Palau is an Island with no terrain (Figure 1c) and it can be considered as an open ocean in the western Pacific. Both Palau and Taiwan are influenced by western north Pacific monsoon (Murakami & Matsumoto, 1994). In the summer season (June to August), southwesterly monsoon flow prevails over these two stations (Chen & Chen, 2003; Kubota et al., 2005). Precipitation of a given location will enhance if it is surrounded by terrain (Houze, 2012). For instance, simulated results of Kirshbaum and Smith (2009) showed that a moist moderately unstable layer of air grows to vigorously intensifying clouds once it carried over the terrain by prevailing winds. The upslope cross-barrier southwesterly flow over northwest of Taiwan will lift the deep layer of very unstable air to above its level of free convection. With the enhanced instability, the clouds extended to deeper altitudes over the windward side of CMR (Houze, 2012). This result in intense precipitation over Taiwan (NCU) when compared to Palau station. To confirm the above statement, the convective available potential energy (CAPE) values for the JWD measured summer season rainy days (excluding typhoon rainy days) over Taiwan (NCU; 24.375° – 25.5°N, 120.625°–121.75°E) and Palau (6.75°–7.875°N, 133.875°–135°E) stations are obtained from ERA-Interim and are depicted with box and whisker plot in Figure 10. In Figure 10, the centerline of the box indicates the median, and the bottom and top lines of the box indicate the 25th and 75th percentiles, respectively. The bottom and top of the dashed vertical lines indicate the 5th and 95th percentiles, respectively. The plus marks in Figure 10 represent outliers of CAPE values. It is apparently seen from the figure that the summer precipitation of NCU has higher CAPE values than Palau. This clearly suggests that the precipitating clouds over Taiwan station (NCU) are more convective than Palau station with more vigorous updrafts and downdrafts. The storm and bright band heights for the JWD measured rainy days over the observational sites of Taiwan (NCU; 24°–25.2°N, 121°–121.9°E) and Palau (6.7°–7.7°N, 133.78°–134.78°E) are obtained from TRMM 2A23 data product and are provided in Figure 11. From the Figure 11 it is apparent that the low storm heights (< 4 km) and bright band heights are dominated over Palau observational site than Taiwan observational site (NCU). The deeper the extent of clouds, the more ice/liquid particles grow to bigger size. The cloud effective radii (CER) of liquid and ice particles for the JWD measured rainy days over Taiwan (NCU; 24.375° – 25.5°N, 120.625°–121.75°E) and Palau (6.75°–7.875°N, 133.875°–135°E) stations are acquired from the level 3 data product (MOD08\_D3) of MODIS, and these values are plotted in Figure 12. Interestingly, we can notice higher CER of ice and water over observational site of Palau than Taiwan (NCU). This could be due to more aerosol loading over Taiwan when compared to Palau. Both local and long-range transported aerosols from southeast China are the major source of aerosols over Taiwan (Wang et al., 2010). It was well documented in the literature

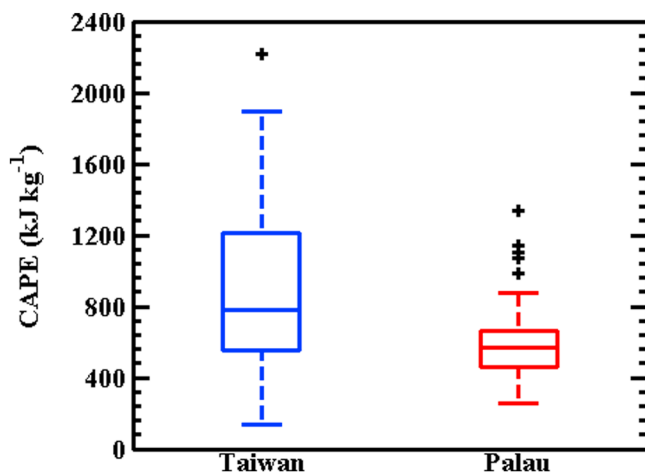


**Figure 10.** Box and whisker plot of convective available potential energy (CAPE,  $\text{kJ kg}^{-1}$ ) for Taiwan (blue color box) and Palau (red color box) regions. The centerline of the box indicates the median, and the bottom and top lines of the box indicate the 25th and 75th percentiles, respectively. The bottom and top of the dashed vertical lines indicate the 5th and 95th percentiles, respectively. The outliers are represented with plus symbols.

indicate the 5th and 95th percentiles, respectively. The plus marks in Figure 10 represent outliers of CAPE values. It is apparently seen from the figure that the summer precipitation of NCU has higher CAPE values than Palau. This clearly suggests that the precipitating clouds over Taiwan station (NCU) are more convective than Palau station with more vigorous updrafts and downdrafts. The storm and bright band heights for the JWD measured rainy days over the observational sites of Taiwan (NCU; 24°–25.2°N, 121°–121.9°E) and Palau (6.7°–7.7°N, 133.78°–134.78°E) are obtained from TRMM 2A23 data product and are provided in Figure 11. From the Figure 11 it is apparent that the low storm heights (< 4 km) and bright band heights are dominated over Palau observational site than Taiwan observational site (NCU). The deeper the extent of clouds, the more ice/liquid particles grow to bigger size. The cloud effective radii (CER) of liquid and ice particles for the JWD measured rainy days over Taiwan (NCU; 24.375° – 25.5°N, 120.625°–121.75°E) and Palau (6.75°–7.875°N, 133.875°–135°E) stations are acquired from the level 3 data product (MOD08\_D3) of MODIS, and these values are plotted in Figure 12. Interestingly, we can notice higher CER of ice and water over observational site of Palau than Taiwan (NCU). This could be due to more aerosol loading over Taiwan when compared to Palau. Both local and long-range transported aerosols from southeast China are the major source of aerosols over Taiwan (Wang et al., 2010). It was well documented in the literature

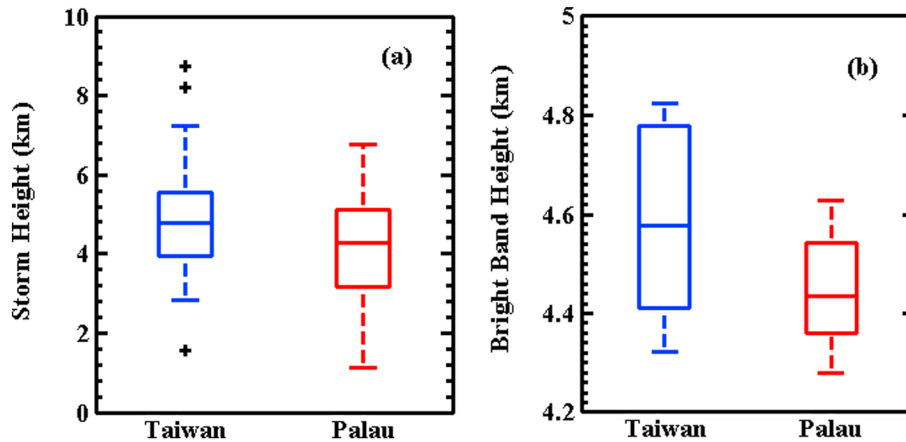


Figure 11. Box and whisker plots of (a) storm height and (b) bright band height for Taiwan (blue color box) and Palau (red color box) regions.

that the aerosols can act as cloud condensation nuclei, increasing the number of cloud droplets and reduces the effective size of the cloud particles (Breon et al., 2002). This characteristic is confirmed by the higher aerosol optical depth (AOD) over Taiwan when compared to Palau (Figure 13). Figure 13 is also drawn by considering the AOD for the JWD measured rainy days over Taiwan (NCU; 24.375° – 25.5°N, 120.625°–121.75°E) and Palau (6.75°–7.875°N, 133.875°–135°E) stations from level 3 data product of MODIS. Rangno and Hobbs (2005) noticed the least influence of aerosols on the subcloud layer on the height above the cloud base in the Marshall Islands. With the least influence of aerosols over the oceanic station (Palau), the CER of ice and water are larger as compared to Taiwan (NCU). By using satellite measurements, Breon et al. (2002) also found larger cloud droplet size over remote tropical oceans and smaller cloud droplet size over highly polluted continental areas. Present CER values over polluted station (NCU) and remote oceanic station (Palau) revealed the similar characteristics to that of Breon et al. (2002).

Strong convective activity extends the clouds to deeper altitudes results in cold rain process with faster growth of ice crystals above the melting layer. The strong updrafts carry the small drops to higher altitudes and thereby allowing bigger drops to precipitate locally. Middle drops grow at the expense of suspended small drops at higher altitudes. Drop sorting and evaporation process attribute to the less number of small drops in heavy precipitation (Atlas et al., 2000; Sauvageot & Lacaux, 1995). Because of relatively higher CAPE values over the observational site of Taiwan (NCU) than Palau (Figure 10), one could expect more large drops at NCU than Palau by the above mentioned processes. In deep stratiform clouds, the ice crystals have sufficient time to grow as larger snowflakes by one or more of the growth modes (vapor deposition, aggregation, and riming), and these large snowflakes transform to relatively large drops once they cross the melting layer. Because of the sufficiently higher bright band over Taiwan (NCU), aggregation and riming

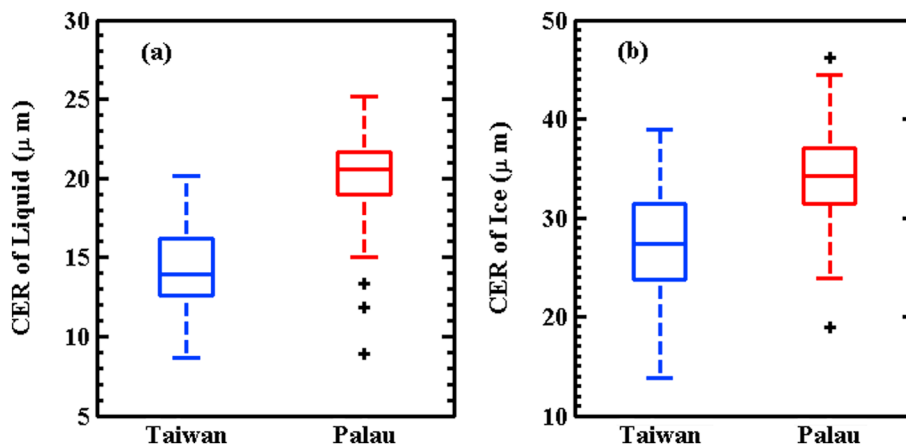
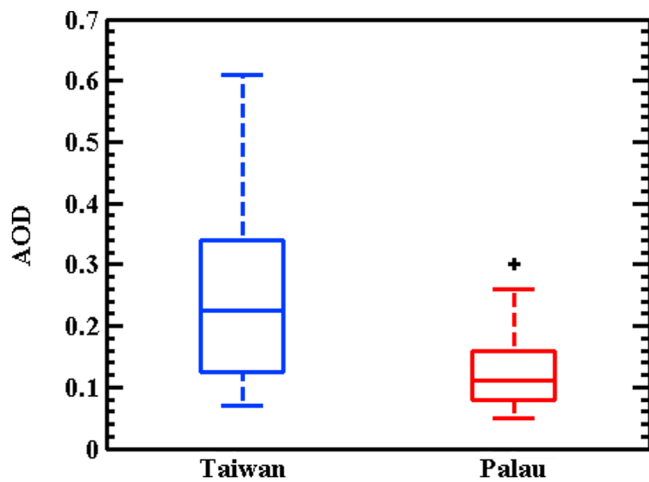


Figure 12. Box and whisker plots of cloud effective radius (CER,  $\mu\text{m}$ ) of (a) liquid and (b) ice particles over Taiwan (blue color box) and Palau (red color box) regions.



**Figure 13.** Box and whisker plot of aerosol optical depth (AOD) for Taiwan (blue color box) and Palau (red color box) regions.

process above the melting layer and drop sorting and collision-coalescence process below the melting layer result in bigger drops at the ground (Heymsfield et al., 2002; Medina & Houze, 2003; Rosenfeld & Ulbrich, 2003; Yuter & Houze, 2003). The dominant low storm heights (< 4 km) over Palau (Figure 11a) confirm that the most of the precipitating clouds over Palau are associated with warm rain process, in which collision-coalescence is the dominant process. The relatively large size of cloud droplets over Palau (Figure 12) is favorable for the collision-coalescence process between the cloud droplets and raindrops, which results in precipitation with more small drops and thus generating smaller  $D_m$  and higher  $N_w$  values. A lower concentration of cloud condensation nuclei (CCN) and cloud droplet concentration result in broad droplet size spectra through the collision-coalescence process. Whereas if the concentration of CCN and cloud droplets are high, the droplet-size spectra are narrow (Wallace & Hobbs, 1977). The higher aerosol concentration (Figure 13) over Taiwan (NCU) inhibits the collision-coalescence processing (suppresses warm rain process), increases the number of cloud droplets, and decreases their effective radius (Figure 12), leading to narrow

droplet size spectra (Albrecht, 1989; Rosenfeld, 1999; Twomey, 1977). More aerosols (Figure 13) over Taiwan (NCU) delay the precipitation above the melting layer, and this delay in precipitation provides sufficient time for the conversion of liquid particles to ice hydrometeors. This conversion can be due to contact nucleation or homogeneous freezing (Wang, 2013). The latent heat released during the ice hydrometeor conversion can upturn the convective activity (showing higher CAPE values over Taiwan in Figure 10) (Khain et al., 2005; Lee et al., 2010; Rosenfeld et al., 2008). Low aerosol concentration over Palau (Figure 13) increase the size of the cloud droplets (Figure 12) through the collision-coalescence process, which results in broad droplet size spectra. As the most of the precipitating clouds over Palau are of warm clouds (lower storm heights, Figure 11), aerosols have the least influence on the vertical development of precipitation clouds (an increase of cloud top heights) over Palau (Li et al., 2011). In terrain-influenced precipitation, the windward slope has heavily rimed particles fall out (Hobbs et al., 1973). Increase in the collision-coalescence process is aided by strong updraft by holding the small drops aloft result in large  $D_m$  over Taiwan when compared to Palau rainfall. Similar results were noticed by May et al. (2011) over Darwin, and they showed that thunderstorm with higher aerosols concentration has lower  $N_w$  and large median volume diameter ( $D_o$ ) when compared to thunderstorms with lower aerosol concentration.

## 5. Summary and Conclusions

For the first time, by using five years of JWD data, RSD variability in summer season rainfall between two islands (Palau and Taiwan) in western Pacific region are studied. In addition to JWD measurements, reanalysis (ERA-Interim) and remote sensing (TRMM and MODIS) data sets are used to illustrating the possible dynamical and microphysical process that occurred at these two locations. This study provides a unique opportunity in understanding the rain microphysics responsible for the RSD variations between oceanic station to that of a terrain surrounded station in western Pacific region. The main conclusions drawn from the current study are as follows:

1. Palau rainfall has a higher concentration of small drops when compared to Taiwan rainfall.
2. Normalized raindrop spectra of Taiwan and Palau rainfall showed a clear demarcation, which clearly indicates that the RSD evolution at these two stations is involved with different microphysical processes.
3. RSD Stratification by rain rate showed a higher concentration of mid and large drops in Taiwan rainfall than that of Palau. Taiwan has a higher mass-weighted mean diameter ( $D_m$ ) and a lower normalized intercept parameter ( $N_w$ ), slope parameter ( $\Lambda$ ), shape parameter ( $\mu$ ) than Palau.
4. Classification of summer rainfall into stratiform and convective regimes showed a lower concentration of small drops, and a higher concentration of middle and large drops at Taiwan's station than Palau's station in both the rainfall regimes (stratiform and convective). The mass-weighted mean diameter ( $D_m$ ) of Palau's convective rainfall is deviated from the maritime-like convective  $D_m$  of Bringi et al. (2003), whereas Taiwan's convective  $D_m$  is similar to the maritime-like convective  $D_m$  of Bringi et al. (2003).

5. The radar reflectivity-rain rate ( $Z-R$ ) relations are found to be different between Palau and Taiwan rainfall.
6. Significant differences in CAPE, storm heights, bright band heights, CER, and AOD are found between precipitation at Palau and Taiwan observational sites.

The present study suggests that both orography and aerosol loading are responsible for the spatial variability of RSD over western Pacific region. The results achieved in this study affords a physical basis in improving the remote-/ground-based radar rainfall retrieval algorithms and in cloud microphysics parameterization in numerical models.

#### Acknowledgments

We are thankful to Japan Agency for Marine-Earth Science and Technology (JAMSTEC), Japan, for providing the disdrometer data at Palau. We acknowledge the Japan Aerospace Exploration Agency (JAXA), Tropical Rainfall Measuring Mission (TRMM), ERA-Interim, and MODIS for providing the data. We are thankful to the Ministry of Science and Technology (MOST), Taiwan for supporting this research work under grants MOST 104-2923-M-008-003-MY5 and MOST 106-2625-M-008-013. The first author, Balaji Kumar Seela (B. K. S.), acknowledges Academia Sinica, Taiwan, for providing graduate fellowship under Taiwan International Graduate Program (TIGP). B. K. S. also acknowledges Ministry of Science and Technology (MOST), Taiwan, for providing the travel support under the grant MOST-106-2922-I-008-041. Second author, J. Jayalakshmi, acknowledges the Ministry of Science and Technology (MOST), Taiwan, R.O.C to carry out this research work under grants MOST 104-2811-M-008-064 and MOST 106-2811-M-008-084. The authors are thankful to the Editor and two anonymous reviewers for their constructive comments and suggestions that helped in improving the manuscript. The JWD data for the Taiwan station are available by contacting the corresponding author (tliam@pblap.atm.ncu.edu.tw). The JWD data for the Palau station can be obtained by contacting the coauthor (Ryuichi Shirooka; shiro@jamstec.go.jp). The TRMM-PR 2A23 data product are obtained from the NASA Goddard Earth Sciences Data and Information Services Center (<https://pmm.nasa.gov/data-access/downloads/trmm>). MODIS level 3 data product (MOD08\_D3) are provided by NASA Goddard space flight center ([https://modaps.modaps.eosdis.nasa.gov/services/about/products/c6/MOD08\\_D3.html](https://modaps.modaps.eosdis.nasa.gov/services/about/products/c6/MOD08_D3.html)). The ERA-Interim data products can be obtained from <http://apps.ecmwf.int/datasets/data/interim-full-daily/levtype=sfc/>.

#### References

- Albrecht, B. A. (1989). Aerosols, cloud microphysics and fractional cloudiness. *Science*, 245(4923), 1227–1230. <https://doi.org/10.1126/science.245.4923.1227>
- Angulo-Martinez, M., & Barros, A. P. (2015). Measurement uncertainty in rainfall kinetic energy and intensity relationships for soil erosion studies: An evaluation using PARSIVEL disdrometers in the Southern Appalachian Mountains. *Geomorphology*, 228, 28–40. <https://doi.org/10.1016/j.geomorph.2014.07.036>
- Atlas, D., Ulbrich, C. W., Marks, F. D. Jr., Amitai, E., & Williams, C. R. (1999). Systematic variation of drop size and radar-rainfall relations. *Journal of Geophysical Research*, 104(D6), 6155–6169. <https://doi.org/10.1029/1998JD200098>
- Atlas, D., Ulbrich, C. W., Marks, F. D. Jr., Black, R. A., Amitai, E., Willis, P. T., & Samsury, C. E. (2000). Partitioning tropical oceanic convective and stratiform rains by draft strength. *Journal of Geophysical Research*, 105(D2), 2259–2267. <https://doi.org/10.1029/1999JD901009>
- Atlas, D., & Williams, C. R. (2003). The anatomy of a continental tropical convective storm. *Journal of the Atmospheric Sciences*, 60(1), 3–15. [https://doi.org/10.1175/1520-0469\(2003\)060%3C0003:TAOACT%3E2.0.CO;2](https://doi.org/10.1175/1520-0469(2003)060%3C0003:TAOACT%3E2.0.CO;2)
- Awaka, J., Iguchi, T., Kumagai, H., & Okamoto, K. (1997). Rain type classification algorithm for TRMM precipitation radar. In *Proc. 1997 Int. Geoscience and Remote Sensing Symp.* (pp. 1633–1635). Singapore: IEEE.
- Awaka, J., Iguchi, T., & Okamoto, K. (1998). Early results on rain type classification by the Tropical Rainfall Measuring Mission (TRMM) precipitation radar. In *Proc. 8th URSI Commission F Open Symp.* (pp. 143–146). Aveiro, Portugal.
- Awaka, J., Iguchi, T., & Okamoto, K. (2009). TRMM PR standard algorithm 2A23 and its performance on bright band detection. *Journal of the Meteorological Society of Japan*, 87(A), 31–52.
- Badron, K., Ismail, A. F., Din, J., & Tharek, A. R. (2011). Rain induced attenuation studies for V-band satellite communication in tropical region. *Journal of Atmospheric and Solar: Terrestrial Physics*, 73(5–6), 601–610. <https://doi.org/10.1016/j.jastp.2010.12.006>
- Baeck, M. L., & Smith, J. A. (1998). Rainfall estimation by the WSR-88D for heavy rainfall events. *Weather Forecasting*, 13(2), 416–436. [https://doi.org/10.1175/1520-0434\(1998\)013%3C0416:REBTWF%3E2.0.CO;2](https://doi.org/10.1175/1520-0434(1998)013%3C0416:REBTWF%3E2.0.CO;2)
- Battan, L. J. (1973). *Radar observation of the atmosphere*, (324 p.). Chicago: University of Chicago Press.
- Boodoo, S., Hudak, D., Ryzhkov, A., Zhang, P., Donaldson, N., Sills, D., & Reid, J. (2015). Quantitative precipitation estimation from a C-band dual-polarized radar for the 8 July 013 flood in Toronto, Canada. *Journal of Hydrometeorology*, 16(5), 2027–2044. <https://doi.org/10.1175/JHM-D-15-0003.1>
- Breon, F. M., Tanre, D., & Generoso, S. (2002). Aerosol effect on cloud droplet size monitored from satellite. *Science*, 295(5556), 834–838. <https://doi.org/10.1126/science.1066434>
- Bringi, V., Chandrasekar, V., Hubbert, J., Gorgucci, E., Randeu, W. L., & Schoenhuber, M. (2003). Raindrop size distribution in different climatic regimes from disdrometer and dual-polarized radar analysis. *Journal of the Atmospheric Sciences*, 60(2), 354–365. [https://doi.org/10.1175/1520-0469\(2003\)060%3C0354:RSDIDC%3E2.0.CO;2](https://doi.org/10.1175/1520-0469(2003)060%3C0354:RSDIDC%3E2.0.CO;2)
- Bumke, K., & Seltmann, J. (2012). Analysis of measured drop size spectra over land and sea. *ISRN Meteorology*, 2012, 1–10. <https://doi.org/10.5402/2012/296575>
- Cao, Q., Zhang, G., Brandes, E., Schuur, T., Ryzhkov, A., & Ikeda, K. (2008). Analysis of video disdrometer and polarimetric radar to characterize rain microphysics in Oklahoma. *Journal of Applied Meteorology and Climatology*, 47(8), 2238–2255. <https://doi.org/10.1175/2008JAMC1732.1>
- Chakravarty, K., & Maitra, A. (2010). Rain attenuation studies over an earth space path at a tropical location. *Journal of Atmospheric and Solar: Terrestrial Physics*, 72(1), 135–138. <https://doi.org/10.1016/j.jastp.2009.10.018>
- Chapon, B., Delrieu, G., Gosset, M., & Boudevillain, B. (2008). Variability of raindrop size distribution and its effect on the Z-R relationship: A case study for intense Mediterranean rainfall. *Atmospheric Research*, 87(1), 52–65. <https://doi.org/10.1016/j.atmosres.2007.07.003>
- Chen, B., Yang, J., & Pu, J. (2013). Statistical characteristics of raindrop size distribution in the Meiyu season observed in Eastern China. *Journal of the Meteorological Society of Japan*, 91(2), 215–227. <https://doi.org/10.2151/jmsj.2013-208>
- Chen, C. S., & Chen, Y. L. (2003). The rainfall characteristic of Taiwan. *Monthly Weather Review*, 131(7), 1323–1341. [https://doi.org/10.1175/1520-0493\(2003\)131%3C1323:TRCOT%3E2.0.CO;2](https://doi.org/10.1175/1520-0493(2003)131%3C1323:TRCOT%3E2.0.CO;2)
- Chen, T. C., Yen, M. C., Hsieh, J. C., & Arritt, R. W. (1999). Diurnal and seasonal variations of the rainfall measured by the Automatic Rainfall and Meteorological Telemetry System in Taiwan. *Bulletin of the American Meteorological Society*, 80(11), 2299–2312. [https://doi.org/10.1175/1520-0477\(1999\)080%3C2299:DASVOT%3E2.0.CO;2](https://doi.org/10.1175/1520-0477(1999)080%3C2299:DASVOT%3E2.0.CO;2)
- Cohen, C., & McCaul, E. W. Jr. (2006). The sensitivity of simulated convective storms to variations in prescribed single-moment microphysics parameters that describe particle distributions, sizes, and numbers. *Monthly Weather Review*, 134(9), 2547–2565. <https://doi.org/10.1175/MWR3195.1>
- Das, S. K., Konwar, M., Chakravarty, K., & Deshpande, S. M. (2017). Raindrop size distribution of different cloud types over the Western Ghats using simultaneous measurements from Micro-Rain Radar and disdrometer. *Atmospheric Research*, 186(2017), 72–82. <https://doi.org/10.1016/j.atmosres.2016.11.003>
- Dee, D. P., Uppala, S. M., Simmons, A. J., Berrisford, P., Poli, P., Kobayashi, S., ... Vitart, F. (2011). The ERA-interim reanalysis: Configuration and performance of the data assimilation system. *Quarterly Journal of the Royal Meteorological Society*, 137(656), 553–597. <https://doi.org/10.1002/qj.828>
- Fadnavis, S., Deshpande, M., Ghude, S. D., & Raj, P. E. (2014). Simulation of severe thunder storm event: A case study over Pune, India. *Natural Hazards*, 72(2), 927–943. <https://doi.org/10.1007/s11069-014-1047-1>
- Gatlin, P. N., Thurai, M., Bringi, V. N., Petersen, W., Wolff, D., Tokay, A., ... Wingo, M. (2015). Searching for large raindrops: A global summary of two-dimensional video disdrometer observations. *Journal of Applied Meteorology and Climatology*, 54(5), 1069–1089. <https://doi.org/10.1175/JAMC-D-14-0089.1>

- Gilmore, M. S., Straka, J. M., & Rasmussen, E. N. (2004). Precipitation uncertainty due to variations in precipitation particle parameters with a simple microphysics scheme. *Monthly Weather Review*, 132(11), 2610–2627. <https://doi.org/10.1175/MWR2810.1>
- Gunn, R., & Kinzer, G. D. (1949). The terminal velocity of fall for water droplets in stagnant air. *Journal of Meteorology*, 6, 233–248.
- Harikumar, R. (2016). Orographic effect on tropical rain physics in the Asian monsoon region. *Atmospheric Science Letters*, 17(10), 556–563. <https://doi.org/10.1002/asl.692>
- Heymsfield, A. J., Bansemmer, A., Field, P. R., Durden, S. L., Stith, J. L., Dye, J. E., ... Grainger, C. A. (2002). Observations and parameterizations of particle size distributions in deep tropical cirrus and stratiform precipitating clouds: Results from in situ observations in TRMM field campaigns. *Journal of the Atmospheric Sciences*, 59(24), 3457–3491. [https://doi.org/10.1175/1520-0469\(2002\)059%3C3457:OAPOPS%3E2.0.CO;2](https://doi.org/10.1175/1520-0469(2002)059%3C3457:OAPOPS%3E2.0.CO;2)
- Hobbs, P. V., Easter, R. C., & Fraser, A. B. (1973). A theoretical study of the flow of air and fallout of solid precipitation over mountainous terrain: Part II. Microphysics. *Journal of the Atmospheric Sciences*, 30(5), 813–823. [https://doi.org/10.1175/1520-0469\(1973\)030%3C0813:ATSOTF%3E2.0.CO;2](https://doi.org/10.1175/1520-0469(1973)030%3C0813:ATSOTF%3E2.0.CO;2)
- Hou, A., Jackson, G. S., Kummerow, C., & Shepherd, C. M. (2008). In S. Michaelides (Ed.), *Global precipitation measurement. Precipitation: Advances in measurement, estimation, and prediction*, (pp. 131–169). Berlin: Springer. [https://doi.org/10.1007/978-3-540-77655-0\\_6](https://doi.org/10.1007/978-3-540-77655-0_6)
- Houze, R. A. Jr. (2012). Orographic effects on precipitating clouds. *Reviews of Geophysics*, 50, RG1001. <https://doi.org/10.1029/2011RG000365>
- Hu, Z., & Srivastava, R. C. (1995). Evolution of raindrop size distribution by coalescence, breakup, and evaporation: Theory and observation. *Journal of the Atmospheric Sciences*, 52(10), 1761–1783. [https://doi.org/10.1175/1520-0469\(1995\)052%3C1761:EOSRDB%3E2.0.CO;2](https://doi.org/10.1175/1520-0469(1995)052%3C1761:EOSRDB%3E2.0.CO;2)
- Iguchi, T., Kozu, T., Meneghini, R., Awaka, J., & Okamoto, K. (2000). Rain-profiling algorithm for the TRMM precipitation radar. *Journal of Applied Meteorology*, 39(12), 2038–2052. [https://doi.org/10.1175/1520-0450\(2001\)040%3C2038:RPAFTT%3E2.0.CO;2](https://doi.org/10.1175/1520-0450(2001)040%3C2038:RPAFTT%3E2.0.CO;2)
- Jayalakshmi, J., & Reddy, K. K. (2014). Raindrop size distributions of southwest and northeast monsoon heavy precipitations observed over Kadapa (14°4'N, 78°82'E), a semi-arid region of India. *Current Science*, 107(8), 1312–1320.
- Joss, J., & Waldvogel, A. (1969). Raindrop size distribution and sampling size errors. *Journal of the Atmospheric Sciences*, 26(3), 566–569. [https://doi.org/10.1175/1520-0469\(1969\)026%3C0566:RSDASS%3E2.0.CO;2](https://doi.org/10.1175/1520-0469(1969)026%3C0566:RSDASS%3E2.0.CO;2)
- Jung, S. A., Lee, D.-I., Jou, B. J.-D., & Uyeda, H. (2012). Microphysical properties of maritime squall line observed on June 2, 2008 in Taiwan. *Journal of the Meteorological Society of Japan*, 90(5), 833–850. <https://doi.org/10.2151/jmsj.2012-516>
- Kerns, B. W. J., Chen, Y. L., & Chang, M. Y. (2010). The diurnal cycle of winds, rain, and clouds over Taiwan during the Mei-Yu, summer, and autumn rainfall regimes. *Monthly Weather Review*, 138(2), 497–516. <https://doi.org/10.1175/2009MWR3031.1>
- Khain, A., Rosenfeld, D., & Pokrovsky, A. (2005). Aerosol impact on the dynamics and microphysics of deep convective clouds. *Quarterly Journal of the Royal Meteorological Society*, 131(611), 2639–2663. <https://doi.org/10.1256/qj.04.62>
- King, M. D., Menzel, W. P., Kaufman, Y. J., Tanre, D., Gao, B.-C., Platnick, S., ... Hubanks, P. A. (2003). Cloud and aerosol properties, precipitable water, and profiles of temperature and water vapor. *IEEE Transactions on Geoscience and Remote Sensing*, 41(2), 442–458. <https://doi.org/10.1109/TGRS.2002.808226>
- Kirshbaum, D. J., & Smith, R. B. (2009). Orographic precipitation in the tropics: Large-eddy simulations and theory. *Journal of the Atmospheric Sciences*, 66(9), 2559–2578. <https://doi.org/10.1175/2009JAS2990.1>
- Kozu, T., Iguchi, T., Kubota, T., Yoshida, N., Seto, S., Kwiatkowski, J., & Takayabu, Y. N. (2009). Feasibility of raindrop size distribution parameter estimation with TRMM precipitation radar observations of shallow convection with a rain cell model. *Journal of the Meteorological Society of Japan*, 87A, 53–66. <https://doi.org/10.2151/jmsj.87A.53>
- Kozu, T., Reddy, K. K., Mori, S., Thurai, M., Ong, J. T., & Rao, D. N. (2006). Seasonal and diurnal variations of raindrop size distribution in Asian monsoon region. *Journal of the Meteorological Society of Japan*, 84A, 195–209. <https://doi.org/10.2151/jmsj.84A.195>
- Kozu, T., Shimomai, T., & Kashiwagi, N. (2009). Raindrop size distribution modeling from a statistical rain parameter relation and its application to the TRMM precipitation radar rain retrieval algorithm. *Journal of Applied Meteorology and Climatology*, 48(4), 716–724. <https://doi.org/10.1175/2008JAMC1998.1>
- Krishna, U. V. M., Reddy, K. K., Seela, B. K., Shirooka, R., Lin, P.-L., & Pan, C.-J. (2016). Raindrop size distribution of easterly and westerly monsoon precipitation observed over Palau islands in the Western Pacific Ocean. *Atmospheric Research*, 174, 41–51. <https://doi.org/10.1016/j.atmosres.2016.01.013>
- Kubota, H., Shirooka, R., Ushiyama, T., Chuda, T., Iwasaki, S., & Takeuchi, K. (2005). Seasonal variations of precipitation properties associated with the monsoon over Palau in the western Pacific. *Journal of Hydrometeorology*, 6(4), 518–531. <https://doi.org/10.1175/JHM432.1>
- Kumar, L. S., Lee, Y. H., & Ong, J. T. (2010). Truncated gamma drop size distribution models for rain attenuation in Singapore. *IEEE Transactions on Antennas and Propagation*, 58(4), 1325–1335. <https://doi.org/10.1109/TAP.2010.2042027>
- Kummerow, C., Hong, Y., Olson, W. S., Yang, S., Adler, R. F., McCollum, J., ... Wilheit, T. T. (2001). The evolution of the Goddard profile algorithm (GPROF) for rainfall estimation from passive microwave sensors. *Journal of Applied Meteorology*, 40(11), 1801–1820. [https://doi.org/10.1175/1520-0450\(2001\)040%3C1801:TEOTGP%3E2.0.CO;2](https://doi.org/10.1175/1520-0450(2001)040%3C1801:TEOTGP%3E2.0.CO;2)
- Lee, G., & Zawadzki, I. (2005). Variability of drop size distributions: Noise and noise filtering in disdrometric data. *Journal of Applied Meteorology*, 44(5), 634–652. <https://doi.org/10.1175/JAM2222.1>
- Lee, S. S., Donner, L. J., & Penner, J. E. (2010). Thunderstorm and stratocumulus: How does their contrasting morphology affect their interactions with aerosols? *Atmospheric Chemistry and Physics*, 10(14), 6819–6837. <https://doi.org/10.5194/acp-10-6819-2010>
- Li, Z., Niu, F., Fan, J., Liu, Y., Rosenfeld, D., & Ding, Y. (2011). The long-term impacts of aerosols on the vertical development of clouds and precipitation. *Nature Geoscience*, 4(12), 888–894. <https://doi.org/10.1038/ngeo1313>
- Liao, L., Meneghini, R., & Tokay, A. (2014). Uncertainties of GPM DPR rain estimates caused by DSD parameterizations. *Journal of Applied Meteorology and Climatology*, 53(11), 2524–2537. <https://doi.org/10.1175/JAMC-D-14-0003.1>
- Marzuki, M., Hashiguchi, H., Yamamoto, M. K., Mori, S., & Yamanaka, M. D. (2013). Regional variability of raindrop size distribution over Indonesia. *Annales Geophysicae*, 31(11), 1941–1948. <https://doi.org/10.5194/angeo-31-1941-2013>
- Marzuki, M., Kozu, T., Shimomai, T., Randeu, W. L., Hashiguchi, H., & Shibagaki, Y. (2009). Diurnal variation of rain attenuation obtained from measurement of raindrop size distribution in equatorial Indonesia. *IEEE Transactions on Antennas and Propagation*, 57(4), 1191–1196. <https://doi.org/10.1109/TAP.2009.2015812>
- May, P. T., Bringi, V. N., & Thurai, M. (2011). Do we observe aerosol impacts on DSDs in strongly forced tropical thunderstorms? *Journal of the Atmospheric Sciences*, 68(9), 1902–1910. <https://doi.org/10.1175/2011JAS3617.1>
- McFarquhar, G. M., Hsieh, T.-L., Freer, M., Mascio, J., & Jewett, B. F. (2015). The characterization of ice hydrometeor gamma size distributions as volumes in  $N_0-\lambda-\mu$  phase space: Implications for microphysical process modeling. *Journal of the Atmospheric Sciences*, 72(2), 892–909. <https://doi.org/10.1175/JAS-D-14-0011.1>
- McFarquhar, G. M., & List, R. (1993). The effect of curve fits for the disdrometer calibration on raindrop spectra, rainfall rate and radar reflectivity. *Journal of Applied Meteorology*, 32(4), 774–782. [https://doi.org/10.1175/1520-0450\(1993\)032%3C0774:TEOCFF%3E2.0.CO;2](https://doi.org/10.1175/1520-0450(1993)032%3C0774:TEOCFF%3E2.0.CO;2)

- Medina, S., & Houze, R. A. (2003). Air motions and precipitation growth in Alpine storms. *Quarterly Journal of the Royal Meteorological Society*, 129(588), 345–371. <https://doi.org/10.1256/qj.02.13>
- Moteki, Q., Shirooka, R., Kubota, H., Ushiyama, T., Reddy, K. K., Yoneyama, K., ... Chuda, T. (2008). Mechanism of the northward propagation of mesoscale convective systems observed on 15 June 2005 during PALAU2005. *Journal of Geophysical Research*, 113, D14126. <https://doi.org/10.1029/2008JD009793>
- Murakami, T., & Matsumoto, J. (1994). Summer monsoon over the Asian continent and western North Pacific. *Journal of the Meteorological Society of Japan*, 72(5), 719–745. [https://doi.org/10.2151/jmsj1965.72.5\\_719](https://doi.org/10.2151/jmsj1965.72.5_719)
- Nakajima, T., & King, M. D. (1990). Determination of the optical thickness and effective particle radius of clouds from reflected solar radiation measurements, Part I: Theory. *Journal of the Atmospheric Sciences*, 47(15), 1878–1893. [https://doi.org/10.1175/1520-0469\(1990\)047%3C1878:DOTOTA%3E2.0.CO;2](https://doi.org/10.1175/1520-0469(1990)047%3C1878:DOTOTA%3E2.0.CO;2)
- Nakamura, K., & Iguchi, T. (2007). In V. Levizanni, P. Bauer, & F. J. Turk (Eds.), *Dual-wavelength radar algorithm. Measuring precipitation from space*, (pp. 225–234). New York: Springer. [https://doi.org/10.1007/978-1-4020-5835-6\\_18](https://doi.org/10.1007/978-1-4020-5835-6_18)
- Nanko, K., Moskalski, S. M., & Torres, R. (2016). Rainfall erosivity–intensity relationships for normal rainfall events and a tropical cyclone on the US southeast coast. *Journal of Hydrology*, 534, 440–450. <https://doi.org/10.1016/j.jhydrol.2016.01.022>
- Narayana Rao, T., Radhakrishna, B., Nakamura, K., & Rao, N. P. (2009). Differences in raindrop size distribution from southwest monsoon to northeast monsoon at Gadanki. *Quarterly Journal of the Royal Meteorological Society*, 135(643), 1630–1637. <https://doi.org/10.1002/qj.432>
- Narayana Rao, T., Rao, D. N., Mohan, K., & Raghavan, S. (2001). Classification of tropical precipitating systems and associated Z–R relationships. *Journal of Geophysical Research*, 106, 17,699–17,711.
- Niu, S., Jia, X., Sang, J., Liu, X., Lu, C., & Liu, Y. (2010). Distributions of raindrop sizes and fall velocities in a semiarid plateau climate: Convective versus stratiform rains. *Journal of Applied Meteorology and Climatology*, 49(4), 632–645. <https://doi.org/10.1175/2009JAMC2208.1>
- Platnick, S., King, M. D., Ackerman, S. A., Menzel, W. P., Baum, B. A., Riedl, J. C., & Frey, R. A. (2003). The MODIS cloud products: Algorithms and examples from Terra. *IEEE Transactions on Geoscience and Remote Sensing*, 41(2), 459–473. <https://doi.org/10.1109/TGRS.2002.808301>
- Radhakrishna, B., Rao, T. N., Rao, D. N., Rao, N. P., Nakamura, K., & Sharma, A. K. (2009). Spatial and seasonal variability of raindrop size distributions in southeast India. *Journal of Geophysical Research*, 114, D04203. <https://doi.org/10.1029/2008JD011226>
- Raghavan, S. (2003). *Radar meteorology*, (p. 549). Kluwer Academic. <https://doi.org/10.1007/978-94-017-0201-0>
- Rangno, A., & Hobbs, P. (2005). Microstructure and precipitation development in cumulus and small cumulonimbus clouds over the warm pool of the tropical Pacific Ocean. *Quarterly Journal of the Royal Meteorological Society*, 131(606), 639–673. <https://doi.org/10.1256/qj.04.13>
- Remer, L. A., Kaufman, Y. J., Tanré, D., Mattoo, S., Chu, D. A., Martins, J. V., ... Holben, B. N. (2005). The MODIS aerosol algorithm, products and validation. *Journal of the Atmospheric Sciences*, 62(4), 947–973. <https://doi.org/10.1175/JAS3385.1>
- Rosenfeld, D. (1999). TRMM observed first direct evidence of smoke from forest fires inhibiting rainfall. *Geophysical Research Letters*, 26(20), 3105–3108. <https://doi.org/10.1029/1999GL006066>
- Rosenfeld, D., Lohmann, U., Raga, G. B., O'Dowd, C. D., Kulmala, M., Fuzzi, S., ... Andreae, M. O. (2008). Flood or drought: How do aerosols affect precipitation? *Science*, 321(5894), 1309–1313. <https://doi.org/10.1126/science.1160606>
- Rosenfeld, D., & Ulbrich, C. W. (2003). Cloud microphysical properties, processes, and rainfall estimation opportunities. *Meteorological Monographs*, 30(52), 237–258. [https://doi.org/10.1175/0065-9401\(2003\)030%3C0237:CMPPAR%3E2.0.CO;2](https://doi.org/10.1175/0065-9401(2003)030%3C0237:CMPPAR%3E2.0.CO;2)
- Rosewell, C. J. (1986). Rainfall kinetic energy in Eastern Australia. *Journal of Climate and Applied Meteorology*, 25(11), 1695–1701. [https://doi.org/10.1175/1520-0450\(1986\)025%3C1695:RKEIEA%3E2.0.CO;2](https://doi.org/10.1175/1520-0450(1986)025%3C1695:RKEIEA%3E2.0.CO;2)
- Ryzhkov, A. V., & Zrnich, D. S. (1995). Comparison of dual polarization radar estimators of rain. *Journal of Atmospheric and Oceanic Technology*, 12(2), 249–256. [https://doi.org/10.1175/1520-0426\(1995\)012%3C0249:CODPRE%3E2.0.CO;2](https://doi.org/10.1175/1520-0426(1995)012%3C0249:CODPRE%3E2.0.CO;2)
- Sauvageot, H., & Lacaux, J. P. (1995). The shape of averaged drop size distributions. *Journal of the Atmospheric Sciences*, 52(8), 1070–1083. [https://doi.org/10.1175/1520-0469\(1995\)052%3C1070:TSOADS%3E2.0.CO;2](https://doi.org/10.1175/1520-0469(1995)052%3C1070:TSOADS%3E2.0.CO;2)
- Seliga, T. A., & Bringi, V. N. (1976). Potential use of the radar differential reflectivity measurements at orthogonal polarizations for measuring precipitation. *Journal of Applied Meteorology*, 15(1), 69–76. [https://doi.org/10.1175/1520-0450\(1976\)015%3C0069:PUORDR%3E2.0.CO;2](https://doi.org/10.1175/1520-0450(1976)015%3C0069:PUORDR%3E2.0.CO;2)
- Sharma, S., Konwar, M., Sarma, D. K., Kalapureddy, M. C. R., & Jain, A. R. (2009). Characteristics of rain integral parameters during tropical convective, transition and stratiform rain at Gadanki and its application in rain retrieval. *Journal of Applied Meteorology and Climatology*, 48(6), 1245–1266. <https://doi.org/10.1175/2008JAMC1948.1>
- Sheppard, B. E. (1990). Effect of irregularities in the diameter classification of raindrops by the Joss–Waldvogel disdrometer. *Journal of Atmospheric and Oceanic Technology*, 7(1), 180–183. [https://doi.org/10.1175/1520-0426\(1990\)007%3C0180:EOIITD%3E2.0.CO;2](https://doi.org/10.1175/1520-0426(1990)007%3C0180:EOIITD%3E2.0.CO;2)
- Sheppard, B. E., & Joe, P. I. (1994). Comparison of raindrop size distribution measurements by a Joss–Waldvogel disdrometer, a PMS 2DG spectrometer, and a POSS Doppler radar. *Journal of Atmospheric and Oceanic Technology*, 11(4), 874–887. [https://doi.org/10.1175/1520-0426\(1994\)011%3C0874:CORSDM%3E2.0.CO;2](https://doi.org/10.1175/1520-0426(1994)011%3C0874:CORSDM%3E2.0.CO;2)
- Steiner, M., Houze, R. A., & Yuter, S. E. (1995). Climatological characterization of 3-dimensional storm structure from operational radar and rain-gauge data. *Journal of Applied Meteorology*, 34(9), 1978–2007. [https://doi.org/10.1175/1520-0450\(1995\)034%3C1978:CCOTDS%3E2.0.CO;2](https://doi.org/10.1175/1520-0450(1995)034%3C1978:CCOTDS%3E2.0.CO;2)
- Steiner, M., Smith, J. A., & Uijlenhoet, R. (2004). A microphysical interpretation of radar reflectivity–rain rate relationships. *Journal of the Atmospheric Sciences*, 61(10), 1114–1131. [https://doi.org/10.1175/1520-0469\(2004\)061%3C1114:AMIORR%3E2.0.CO;2](https://doi.org/10.1175/1520-0469(2004)061%3C1114:AMIORR%3E2.0.CO;2)
- Tang, Q., Xiao, H., Guo, C., & Feng, L. (2014). Characteristics of the raindrop size distributions and their retrieved polarimetric radar parameters in northern and southern China. *Atmospheric Research*, 135, 59–75.
- Tapiador, F. J., Haddad, Z. S., & Turk, J. (2014). A probabilistic view on raindrop size distribution modeling: A physical interpretation of rain microphysics. *Journal of Hydrometeorology*, 15(1), 427–443. <https://doi.org/10.1175/JHM-D-13-033.1>
- Tenório, R. S., Da Dilva-Moraes, M. C., & Sauvageot, H. (2012). Raindrop size distribution and radar parameters in coastal tropical rain systems of northeastern Brazil. *Journal of Applied Meteorology and Climatology*, 51, 1961–1970.
- Testud, J., Oury, S., Amayenc, P., & Black, R. A. (2001). The concept of “normalized” distributions to describe raindrop spectra: A tool for cloud physics and cloud remote sensing. *Journal of Applied Meteorology*, 40(6), 1118–1140. [https://doi.org/10.1175/1520-0450\(2001\)040%3C1118:TCOND%3E2.0.CO;2](https://doi.org/10.1175/1520-0450(2001)040%3C1118:TCOND%3E2.0.CO;2)
- Thompson, E. J., Rutledge, S. A., Dolan, B., & Thurai, M. (2015). Drop size distributions and radar observations of convective and stratiform rain over the equatorial Indian and West Pacific Oceans. *Journal of the Atmospheric Sciences*, 72(11), 4091–4125. <https://doi.org/10.1175/JAS-D-14-0206.1>
- Thurai, M., Gatlin, P. N., & Bringi, V. N. (2016). Separating stratiform and convective rain types based on the drop size distribution characteristics using 2D video disdrometer data. *Atmospheric Research*, 169, 416–423. <https://doi.org/10.1016/j.atmosres.2015.04.011>
- Tokay, A., Bashor, P. G., Habib, E., & Kasparis, T. (2008). Raindrop size distribution measurements in tropical cyclones. *Monthly Weather Review*, 136(5), 1669–1685. <https://doi.org/10.1175/2007MWR2122.1>

- Tokay, A., Kruger, A., & Krajewski, W. F. (2001). Comparison of drop size distribution measurements by impact and optical disdrometers. *Journal of Applied Meteorology*, 40(11), 2083–2097. [https://doi.org/10.1175/1520-0450\(2001\)040%3C2083:CODSDM%3E2.0.CO;2](https://doi.org/10.1175/1520-0450(2001)040%3C2083:CODSDM%3E2.0.CO;2)
- Tokay, A., & Short, D. A. (1996). Evidence from tropical raindrop spectra of the origin of rain from stratiform versus convective clouds. *Journal of Applied Meteorology*, 35(3), 355–371. [https://doi.org/10.1175/1520-0450\(1996\)035%3C0355:EFTRSO%3E2.0.CO;2](https://doi.org/10.1175/1520-0450(1996)035%3C0355:EFTRSO%3E2.0.CO;2)
- Tokay, A., Wolff, D. B., Wolff, K. R., & Bashor, P. (2003). Rain gauge and disdrometer measurements during the Keys Area Microphysics Project (KAMP). *Journal of Atmospheric and Oceanic Technology*, 20(11), 1460–1477. [https://doi.org/10.1175/1520-0426\(2003\)020%3C1460:RGADM%3E2.0.CO;2](https://doi.org/10.1175/1520-0426(2003)020%3C1460:RGADM%3E2.0.CO;2)
- Twomey, S. (1977). The influence of pollution on the shortwave albedo of clouds. *Journal of the Atmospheric Sciences*, 34(7), 1149–1152. [https://doi.org/10.1175/1520-0469\(1977\)034%3C1149:TIOPOT%3E2.0.CO;2](https://doi.org/10.1175/1520-0469(1977)034%3C1149:TIOPOT%3E2.0.CO;2)
- Ulbrich, C. W. (1983). Natural variations in the analytical form of the raindrop size distribution. *Journal of Climate and Applied Meteorology*, 22(10), 1764–1775. [https://doi.org/10.1175/1520-0450\(1983\)022%3C1764:NVITAF%3E2.0.CO;2](https://doi.org/10.1175/1520-0450(1983)022%3C1764:NVITAF%3E2.0.CO;2)
- Ulbrich, C. W., & Atlas, D. (2007). Microphysics of raindrop size spectra: Tropical continental and maritime storms. *Journal of Applied Meteorology and Climatology*, 46(11), 1777–1791. <https://doi.org/10.1175/2007JAMC1649.1>
- Ushiyama, T., Krishna Reddy, K., Kubota, H., Yasunaga, K., & Shirooka, R. (2009). Diurnal to interannual variation in the raindrop size distribution over Palau in the western tropical Pacific. *Geophysical Research Letters*, 36(2), L02810. <https://doi.org/10.1029/2008GL036242>
- Wainwright, C. E., Dawson, D. T. II, Xue, M., & Zhang, G. (2014). Diagnosing the intercept parameters of the exponential drop size distributions in a single-moment microphysics scheme and impact on supercell storm simulations. *Journal of Applied Meteorology and Climatology*, 53(8), 2072–2090. <https://doi.org/10.1175/JAMC-D-13-0251.1>
- Waldvogel, A. (1974). The  $N_0$  jump of raindrop spectra. *Journal of the Atmospheric Sciences*, 31(4), 1067–1078. [https://doi.org/10.1175/1520-0469\(1974\)031%3C1067:TJORS%3E2.0.CO;2](https://doi.org/10.1175/1520-0469(1974)031%3C1067:TJORS%3E2.0.CO;2)
- Wallace, J. M., & Hobbs, P. V. (1977). *Atmospheric science: An introductory survey*. New York: Academic Press.
- Wang, P. K. (2013). *Physics and dynamics of clouds and precipitation*, (p. 467). New York: Cambridge University Press. <https://doi.org/10.1017/CBO9780511794285>
- Wang, S.-H., Lin, N.-H., Chou, M.-D., Tsay, S.-C., Welton, E. J., Hsu, N. C., ... Holben, B. N. (2010). Profiling transboundary aerosols over Taiwan and assessing their radiative effects. *Journal of Geophysical Research*, 115, D00K31. <https://doi.org/10.1029/2009JD013798>
- Williams, C. R., Ecklund, W. L., & Gage, K. S. (1995). Classification of precipitating clouds in the tropics using 915-MHz wind profilers. *Journal of Atmospheric and Oceanic Technology*, 12(5), 996–1012. [https://doi.org/10.1175/1520-0426\(1995\)012%3C0996:COPCIT%3E2.0.CO;2](https://doi.org/10.1175/1520-0426(1995)012%3C0996:COPCIT%3E2.0.CO;2)
- Yuter, S. E., & Houze, R. A. Jr. (2003). Microphysical modes of precipitation growth determined by S-band vertically pointing radar in orographic precipitation during MAP. *Quarterly Journal of the Royal Meteorological Society*, 129(588), 455–476. <https://doi.org/10.1256/qj.01.216>
- Zwiebel, J., Van Baelen, J., Anquetin, S., Pointin, Y., & Boudevillain, B. (2016). Impacts of orography and rain intensity on rainfall structure. The case of the HyMeX IOP7a event. *Quarterly Journal of the Royal Meteorological Society*, 142, 310–319. <https://doi.org/10.1002/qj.2679>